iScience

CellPress

Article

Obesity Reshapes Visceral Fat-Derived MHC I Associated-Immunopeptidomes and Generates Antigenic Peptides to Drive CD8$^+$ T Cell Responses

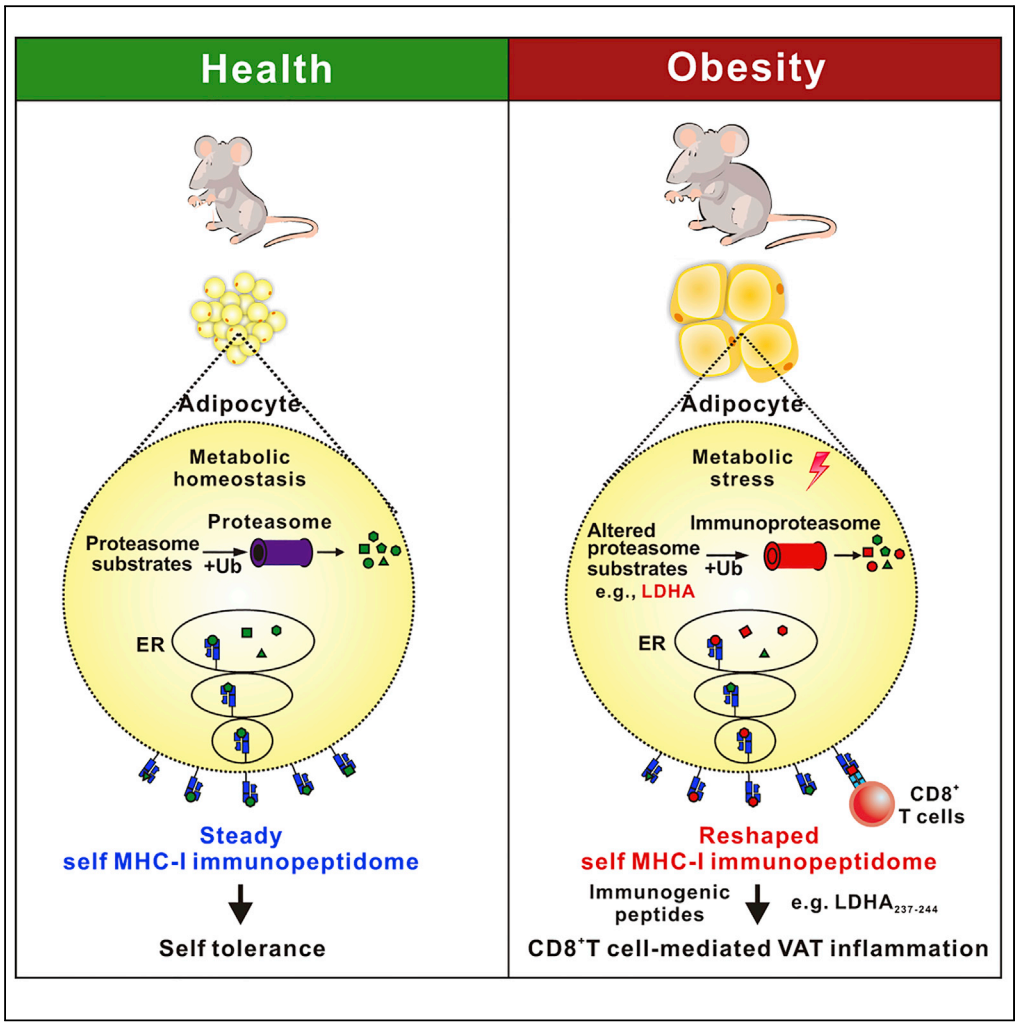

Xiaoling Chen, Shufeng Wang, Yi Huang, ..., Mengjun Zhang, Yuzhang Wu, Li Wang

wuyuzhang@tmmu.edu.cn (Y.W.)
liwang118@icloud.com (L.W.)

HIGHLIGHTS

Obesity reshapes the landscape of VAT-derived MIP

The obese VAT-exclusive MIP reflects an obesity-associated signature

An obese VAT-exclusive peptide LDHA$_{237-244}$ can stimulate CD8$^+$ T cell responses

LDHA$_{237-244}$-reactive CD8$^+$ T cells were present in obese mice but not lean mice

Chen et al., iScience 23, 100977
April 24, 2020
https://doi.org/10.1016/j.isci.2020.100977

iScience

CellPress

Article

Obesity Reshapes Visceral Fat-Derived MHC I Associated-Immunopeptidomes and Generates Antigenic Peptides to Drive CD8$^+$ T Cell Responses

Xiaoling Chen,[1,7] Shufeng Wang,[1,7] Yi Huang,[2] Xia Zhao,[3] Xu Jia,[1,4] Gang Meng,[5] Qian Zheng,[4] Mengjun Zhang,[6] Yuzhang Wu,[1,*] and Li Wang[1,8,*]

SUMMARY

Adaptive CD8$^+$ T cells were observed to contribute to the initiation and progression of obesity-induced visceral adipose tissue (VAT) chronic inflammation that is critically linked to metabolic disorders. Numerous peptides presented by the major histocompatibility complex (MHC) class I molecules at the cell surface are collectively termed as MHC I-associated immunopeptidome (MIP) for the interaction with CD8$^+$ T cells. We conducted the in-depth mapping of MIP of VAT from lean and obese mice using large-scale high-resolution mass spectrometry and observed that obesity significantly alters the landscape of VAT MIPs. Additionally, the obese VAT-exclusive MIP source proteome reflected a distinct obesity-associated signature. A peptide derived from lactate dehydrogenase A (LDHA) or B chain, named LDHA$_{237\text{-}244}$, was identified as an obese VAT-exclusive immunogenic peptide that was capable of eliciting pro-inflammatory CD8$^+$ T cells responses. Our findings suggest that certain immunogenic peptides generated by obesity may trigger CD8$^+$ T cell-mediated VAT inflammation.

INTRODUCTION

The prevalence of obesity and its associated metabolic abnormalities, including insulin resistance, type 2 diabetes mellitus (T2DM), cardiovascular disease (CVD), and non-alcoholic fatty liver disease (NAFLD), has attained epidemic proportions, severely affecting health and global mortality rates. Obesity-induced visceral adipose tissue (VAT) chronic inflammation is now considered to portray a pivotal role in the development of metabolic diseases. Increasing data indicate alterations in multiple immune cells in obese VAT, including alterations in macrophages, mast cells, eosinophils, as well as in adaptive immune cells (Sun et al., 2012). T lymphocytes have been regarded as unexpected contributors to obesity-induced VAT inflammation and insulin resistance (Wu et al., 2007). The inflammatory reaction within obese VAT has been characterized by a striking influx of CD8$^+$ T cells (Rausch et al., 2008). Similarly, the ratio of CD8$^+$ to CD4$^+$ T cells increased in obese VAT weeks before macrophage infiltration (Feuerer et al., 2009; Winer et al., 2009). The infiltration of significant number of CD8$^+$ T cells preceded macrophage recruitment in obese VAT of mice after short-term feeding of a high-fat diet (HFD). Depletion of CD8$^+$ T cells lowered macrophage infiltration and adipose tissue inflammation, and ameliorated systemic insulin resistance, whereas adoptive transfer of CD8$^+$ T cells into CD8-deficient mice reverted these effects and increased the numbers of pro-inflammatory macrophages in VAT (Nishimura et al., 2009). These evidences indicate that CD8$^+$ T cells may portray a significant role in the initiation of obesity-induced VAT inflammation. Obese VAT-infiltrated T cells have a restricted TCR-Vβ repertoire, suggesting that expansion of these T cells in progressive obesity is possibly driven by VAT-specific antigens as a result of obesity (McDonnell et al., 2018; Nishimura et al., 2009; Yang et al., 2010). It has been reported that obese adipose tissue possesses the ability to activate CD8$^+$ T cells, whereas lean fat does not (Nishimura et al., 2009). However, the antigenic mechanisms underlying the activation, proliferation, and pro-inflammatory responses of CD8$^+$ T cells in obese VAT remain unknown.

Numerous peptides presented on the cell surface of major histocompatibility complex (MHC) class I molecules are collectively referred to as the MHC class I-associated immunopeptidome (MIP) interacting with adaptive CD8$^+$ T cells (Granados et al., 2015). Recent studies have adopted large-scale mass spectrometry (MS) as the

[1]Institute of Immunology PLA, Army Medical University (Third Military Medical University), Chongqing 400038, China

[2]Biomedical Analysis Center, Army Medical University (Third Military Medical University), Chongqing 400038, China

[3]Bioinformatics Center, Department of Microbiology, Army Medical University (Third Military Medical University), Chongqing 400038, China

[4]Department of Physiology, North Sichuan Medical College, Nanchong 637007, China

[5]Department of Pathology, Southwest Hospital, Army Medical University (Third Military Medical University), Chongqing 400038, China

[6]Department of Pharmaceutical Analysis, College of Pharmacy, Army Medical University (Third Military Medical University), Chongqing 400038, China

[7]These authors contributed equally

[8]Lead Contact

*Correspondence: wuyuzhang@tmmu.edu.cn (Y.W.), liwang118@icloud.com (L.W.)

https://doi.org/10.1016/j.isci.2020.100977

sole direct approach for analyzing the global composition of MIP. The molecular composition of MIP is complex and varies from one cell/tissue type to another; it is intertwined with protein metabolism and is ultimately shaped by two processes: protein translation and degradation (Adamopoulou et al., 2013; de Verteuil et al., 2010). Under certain pathological conditions, selected intrinsic and extrinsic cellular factors, including neoplastic transformation, infection, as well as metabolic perturbations, can restructure self-MIPs, possibly resulting in the generation of immunogenic peptides (de Verteuil et al., 2012). Malignant transformation has a profound impact on the MIPs. Numerous tumor-associated MIPs have been described to encompass immunogenic peptides that are recognized by $CD8^+$ T cells (Bassani-Sternberg et al., 2016; Boon et al., 2006; Dutoit et al., 2012; Kowalewski et al., 2015; Loffler et al., 2018). Alteration of cellular metabolism via the inhibition of the mammalian target of rapamycin results in dynamic alterations in the cell surface MIP landscape as well as generation of immunogenic peptides (Caron et al., 2011). Additionally, inflammatory cytokines induce the alteration of human β cell MIPs and yield conventional and neo-antigenic peptides recognized by $CD8^+$ T cells in type 1 diabetes and healthy donors (Gonzalez-Duque et al., 2018). However, it remains to be determined whether obesity reshapes VAT-derived MIP and generates immunogenic peptides for driving $CD8^+$ T cell responses. We performed large-scale high-resolution MS to analyze VAT-derived MIPs isolated from lean and obese mice fed a normal chow diet (NCD) and HFD, respectively, and observed that HFD-induced obesity led to significant alterations in the VAT MIP landscape. Moreover, abnormal adipocyte metabolism under obese conditions generated obese VAT-exclusive immunogenic peptides that elicited the pro-inflammatory responses of $CD8^+$ T cells, representing a mechanism underlying the obesity-induced VAT inflammation.

RESULTS

Characterization of MHC Class I-Associated Immunopeptidome Derived from the Visceral Adipose Tissue of NCD-Fed (Lean) and HFD-Fed (Obese) Mice

First, the HFD-induced obese mouse model was well established. HFD-fed obese mice exhibited significantly increased weight and fat mass, along with impaired glucose tolerance and insulin sensitivity (Figures S1A–S1E) at 8 weeks post HFD administration. The epididymal fat pads (VAT samples) freshly harvested from HFD-fed obese mice and NCD-fed lean mice, respectively, were lysed to immunopurify H2-Kb-peptide complexes. Although the mRNA expression level of H2-Kb was lower in obese VAT from HFD-fed mice compared with that from NCD-fed mice, there was no significant difference in H2-Kb protein expression levels in VAT between lean and obese mice (Figures S1F and S1G). The quantity of H2-Kb protein purified from obese VAT was marginally lower than that obtained from lean VAT (Figure S1G). H2-Kb-bound peptides were acid-eluted from the H2-Kb molecules and analyzed using reverse-phase HPLC-tandem mass spectrometry (LC-MS/MS) (Figure 1A). By combining the Mascot and Sequest search results from three technical repetitions, we identified 913 unique peptides from NCD VAT and 404 unique peptides from HFD VAT, which met the following criteria: FDR<5%, either Ionscore >20 in Mascot search or q values < 0.05 in Sequest search, and 8–12 amino acids in length. When applying a more stringent filter using the predicted H2-Kb binding affinity with IC_{50} <500 nM (netMHCpan4.0), we eventually discovered 324 (Table S1. The identified unique high confidence H2-Kb-bound peptides from visceral adipose tissues of NCD-fed mice, related to Figure 1) and 171 (Table S2. The identified unique high confidence H2-Kb-bound peptides from visceral adipose tissues of HFD-fed mice, related to Figure 1) unique high confidence H2-Kb-bound peptides from NCD and HFD VAT, respectively. The two MIP datasets indicated the characteristic length distribution for H2-Kb-restricted peptides, predominantly 8 amino acids in length, with a small number of nonameric peptides and very few of 10- to 11-mer peptides. Notably, the proportion of octapeptides in HFD VAT MIP was higher than that in NCD VAT MIP (Figure 1B). Most of these MIPs (>80%) were predicted to elicit strong H2-Kb binding affinity with IC_{50} < 100 nM (Figure 1C). Similarly, both octapeptides and nonapeptides from the two MIPs exhibited the typical anchor motifs (P5 and P8/9) for H2-Kb molecules binding (Figure 1D). The results confirm the predominant presence of tyrosine and phenylalanine in position P5 and that of leucine, valine, and methionine in the C-terminal positions of peptides. No significant alterations were noted in the amino acid preferences within the MIPs purified from NCD- and HFD VAT. In conjunction, these data indicated that our established VAT MIP datasets were highly reliable. HFD-induced obesity did not change the H2-Kb-binding affinity and the amino acid preferences in MIPs derived from VAT observably; however, it resulted in an increase in the proportion of H2-Kb-bound octameric peptides.

Obesity Reshapes Visceral Adipose Tissue-Derived-MHC Class I-Associated Immunopeptidome

To investigate whether obesity affects the composition of VAT-derived MIP, we overlapped and compared the VAT MIP landscape of NCD- (lean) and HFD-fed (obese) mice (Figure 2A). There were

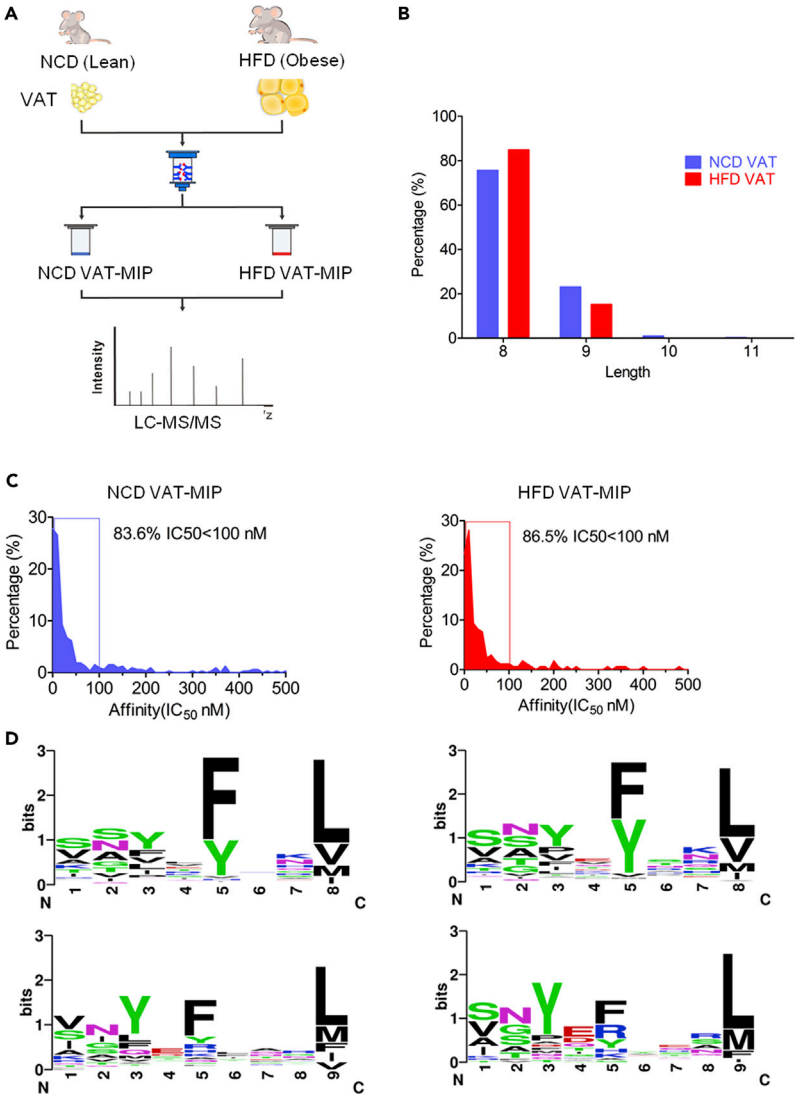

Figure 1. Characterization of MHC Class I-Associated Immunopeptidome (MIP) Derived from the Visceral Adipose Tissue (VAT) of NCD-Fed (Lean) and HFD-Fed (Obese) Mice

(A)Schematic representation of the experimental workflow used to generate and identify VAT MIPs. The epididymal fat pad (VATs) from NCD and HFD-fed C57BL/6 mice were extracted. H2-Kb-associated peptides were isolated independently by immunoaffinity purification using the monoclonal antibodies Y-3, and the eluted peptides were identified using LC-MS/MS.

(B) The column diagram illustrating the length distribution of NCD- and HFD VAT MIPs (8–11 amino acids).

(C) The graphs indicating the distribution of the predicted affinity values of NCD- and HFD VAT MIPs by netMHCpan4.0.

(D) The binding motifs for octameric and nonameric peptides identified in NCD- and HFD VAT MIPs, respectively, were illustrated. The x-axis represents the residue position within octameric and nonameric peptide sequences. The y axis represents the information content, with the size of each amino acid symbol proportional to its frequency.

See also Figure S1 and Tables S1 and S2.

114 H2-Kb-associated peptides shared by both VAT MIPs. HFD VAT MIP had 57 unique peptides (33.33%, Table S3) that were undetected in NCD VAT MIP. The majority (64.81%) of peptides identified in NCD VAT MIP dataset did not exist in the HFD VAT MIP dataset. The NCD VAT MIP and HFD VAT MIP represented 344 and 182 potential source proteins, respectively. Overlaps between the two VAT MIP source proteomes revealed that 126 potential source proteins were shared by MIPs from NCD VAT (36.63%) and HFD VAT (69.23%) samples. Two hundred and eighteen proteins (63.37% of the mapped NCD VAT potential source proteome) were represented exclusively in the NCD VAT MIP. Fifty-six

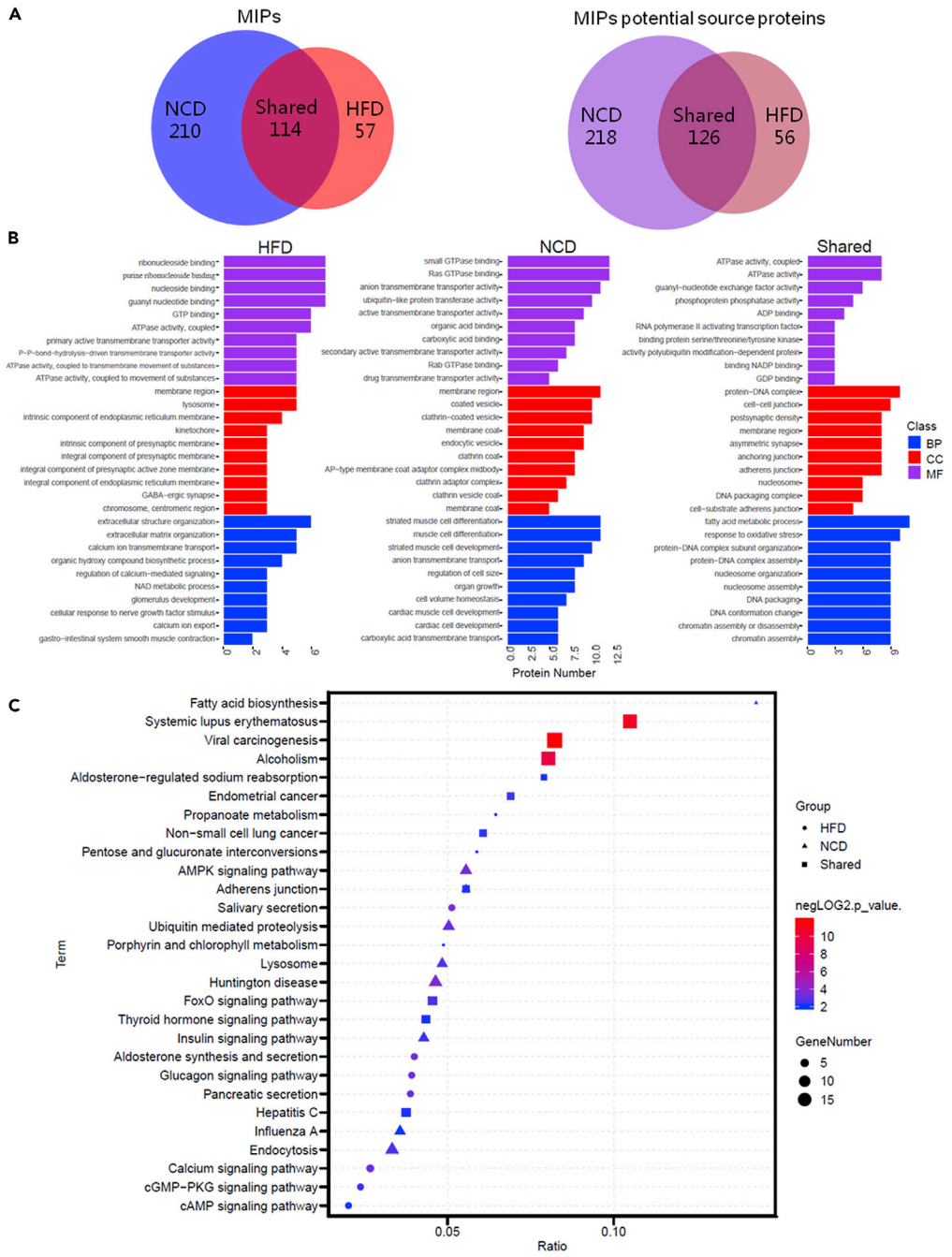

Figure 2. High-Fat Diet-Induced Obesity Reshapes Visceral Adipose Tissue Derived-MHC Class I-Associated Immunopeptidome (MIP)

(A)The Venn diagrams represent the overlap analysis of VAT MIPs and their potential source proteins comparing NCD-fed (lean) and HFD-fed (obese) mice, respectively. Numbers indicate the number of identified peptides or their potential source proteins that were shared between or unique to each MIP.

(B) The top 10 GO enrichment terms of shared or exclusive MIP potential source proteins identified in HFD and NCD VAT. The three GO categories include biological process (BP), molecular function (MF), and cellular component (CC). The x- and y axes represent the protein number of corresponding GO terms and the GO terms, respectively.

(C) KEGG pathway enrichment analysis of shared or exclusive MIP potential source proteins identified in HFD and NCD VAT. The horizontal axis indicates the ratio of the number of identified proteins versus the total number of proteins in the

Figure 2. *Continued*

same KEGG pathway, and the vertical ordinates represent the terms of the KEGG pathways. The bubble size indicates the number of proteins matched in the KEGG pathway. The color represents −log2 (p value): Logarithmic conversion of Fisher exact test p value.

See also Tables S3, S4, and S5.

proteins (30.77% of the mapped HFD VAT potential source proteome) and the 52 corresponding peptides were represented exclusively in the HFD VAT MIP (Table S4).

Next, we mapped the exclusive or shared MIP source proteins from NCD VAT and HFD VAT to the GO enrichment and KEGG pathway enrichment analysis using clusterProfiler. The top 10 statistically significant GO term classification from each group of proteins revealed visibly different clusters in biological process, molecule function, and cellular components among exclusive or shared MIP source proteins from NCD and HFD VAT. Notably, at the biological process level, the shared MIP source protein content was enriched most significantly in fatty acid metabolic processes and response to oxidative stress and nucleosome assembly, whereas the NCD VAT-exclusive MIP source protein content was enriched most significantly in cell volume homeostasis, cardiac muscle cell development, and anion transmembrane transport. The HFD VAT-exclusive MIP source protein content was enriched in extracellular structure organization, NAD metabolic process, calcium ion transmembrane transport, and regulation of calcium-mediated signaling (Figure 2B). The KEGG pathway enrichment analysis further indicated that the NCD and HFD VAT exclusive or shared MIP source protein content was enriched in almost entirely different signaling pathways. Notably, the shared MIP source protein content was significantly enriched in some diseases-related pathways, FoxO signaling pathway, and thyroid hormone signaling pathway; the NCD VAT-exclusive MIP source protein content was enriched in AMPK signaling pathway, ubiquitin-mediated proteolysis, lysosome, endocytosis, and insulin signaling pathway. Both the shared and NCD VAT-exclusive MIP source protein contents were significantly enriched in the adherens junction-related pathways, whereas aldosterone synthesis and secretion, glucagon signaling, calcium signaling, cGMP-PKG signaling, cAMP signaling pathway, pentose and glucuronate interconversions, and pancreatic secretion-related pathway were observed to be enriched in the HFD VAT-exclusive MIP source proteins (Figure 2C). Notably, among the HFD VAT-exclusive MIP source proteins, we observed that a series of proteins, including the lipopolysaccharide-binding protein (LBP), melatonin related receptor (GPR50), and phospholipid transfer protein (PLTP), have been previously reported to be associated with obesity-related chronic inflammation and metabolic disorders (Table S5). These data revealed that obesity reshapes VAT-derived-MIP and the obese VAT-exclusive MIP source proteome reflects a distinct obesity-associated signature.

Selection of Potential Candidate Peptides for Exemplified Immunogenicity Evaluation

We further demonstrated that the increase in $CD8^+$ T cell levels in VAT occurred early and was sustained during the development of HFD-induced obesity (Figures S2A–S2E); hence, we considered whether HFD-induced obesity generates obese VAT-exclusive MHC class I-associated antigenic peptides to drive the pro-inflammatory response of $CD8^+$ T cells. Therefore, we selected several peptides for immunogenicity analysis based on the following selection criteria: obese VAT MIP specificity (on source protein level), significant H2-Kb-affinity, sufficient abundance, and reproducibility (Table S6, G1 and G2). The peptides that were shared by MIP datasets from both HFD VAT and NCD VAT, although these were more abundant in HFD VAT, were selected for the immunogenicity analysis as well (Table S6, G3). First, the H2-Kb molecule binding affinity of the three groups of peptides was determined using the transporter associated with Ag processing (TAP)-deficient RMAS cell-based binding assay. The LCMV GP_{33-41} peptide, a positive control, elicited the highest binding affinity for H2-Kb. Peptides in G1 and G2 exhibited similar medium binding ability, and peptides in G3 exhibited relatively high binding affinity with H2-Kb (Figure 3A). This observation indicated that all groups of peptides have detectable H2-Kb binding abilities. Following this, we evaluated the immunogenicity of these H2-Kb-bound peptides *in vitro* by stimulating splenocytes isolated from C57BL/6 mice with each group of peptide individually and measured $CD8^+$ T cell responses against peptide pool-loaded RMAS cells using intracellular IFN-γ and TNF-α staining (Figure 3B). We observed that peptides in G1 induced pro-inflammatory $CD8^+$ T cell response when restimulated with the corresponding peptides pool-loaded RMAS cells, whereas those in G2 and G3 did not. Moreover, RMAS cells in isolation could not stimulate IFN-γ and TNF-α production by G1 peptide-primed $CD8^+$ T cells, and the $CD8^+$ T cell responses against G1 peptides-loaded RMAS cells were almost completely blocked by anti-H2-Kb antibody Y-3 (Figures 3C–3F).

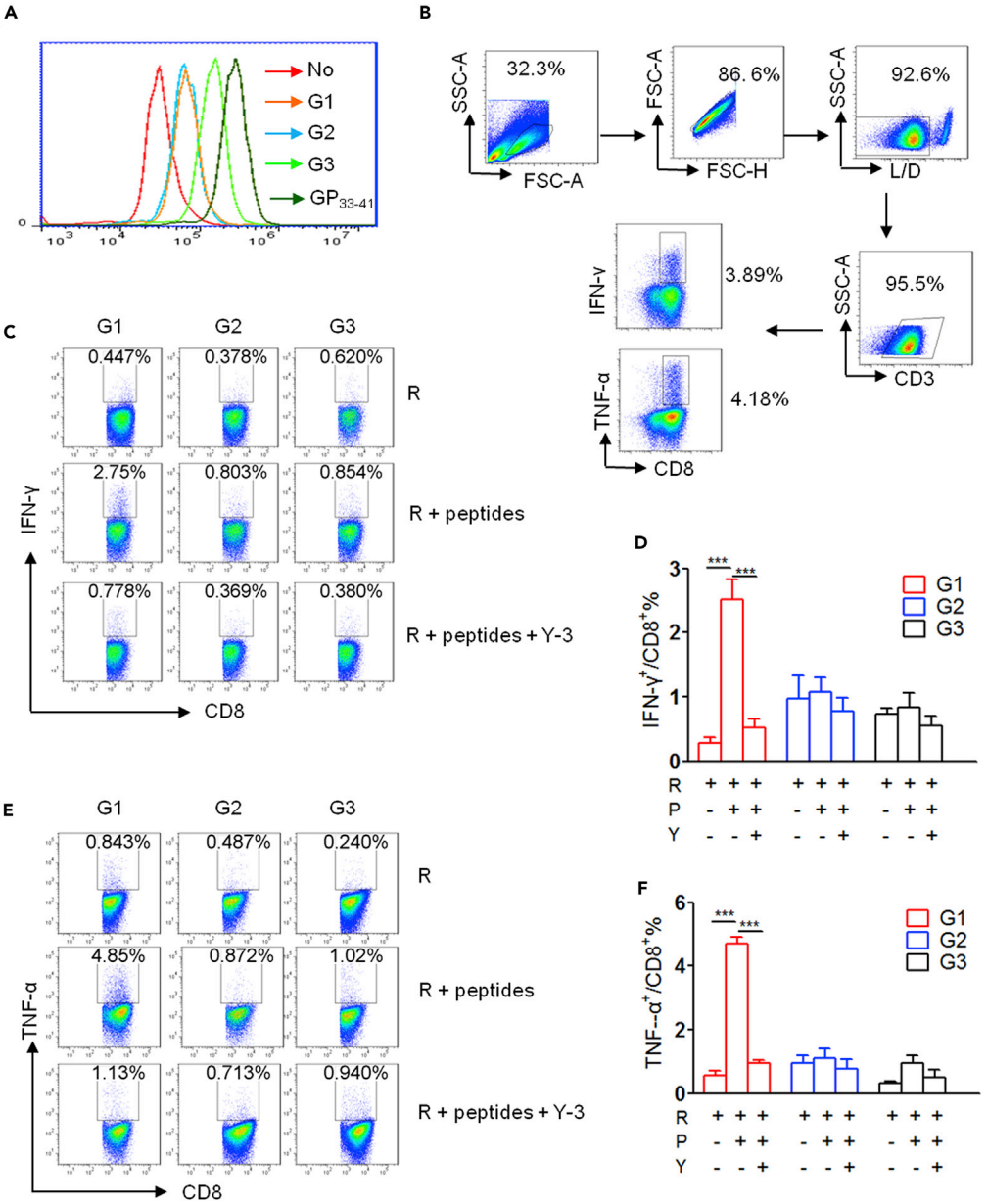

Figure 3. Selection of Potential Candidate Peptides for Exemplified Immunogenicity Evaluation

(A) Representative histogram of FACS analysis of the surface H2-Kb molecules on TAP-deficient RMAS (R) cells incubated with or without the indicated peptide groups.

(B–F) (B) Gating strategy for analysis of intracellular cytokine production by $CD8^+$ T cells. Representative FACS plots indicating intracellular IFN-γ (C) and TNF-α (E) staining of $CD8^+$ T cells restimulated with R alone, or R loaded with the indicated peptide groups, or in the presence of Y-3 antibody. Summary graph for FACS analysis of the frequency of IFN-γ (D) and TNF-α (F)-producing cells among $CD8^+$ T cells stimulated with the indicated peptide group. Each bar represents the mean ± SEM of three independent experiments. ***$p < 0.001$ determined by Student's t test.

See also Figure S2 and Table S6.

Furthermore, the immunogenicity of peptides in G1 was assessed in detail by priming the splenocytes with the respective single peptide, and the splenocyte cultures were then restimulated with peptide-pulsed RMAS cells or RMAS cells alone to determine peptide-specific $CD8^+$ T cell responses using intracellular IFN-γ and TNF-α staining (Figure 4). Among peptides in G1, $DHB12_{16\text{-}24}$, with 17-beta-hydroxys-teroid dehydrogenase 12 (DHB12 or Hsd17b12) as its source protein, stimulated a weak peptide-specific $CD8^+$ T cell response. Notably,

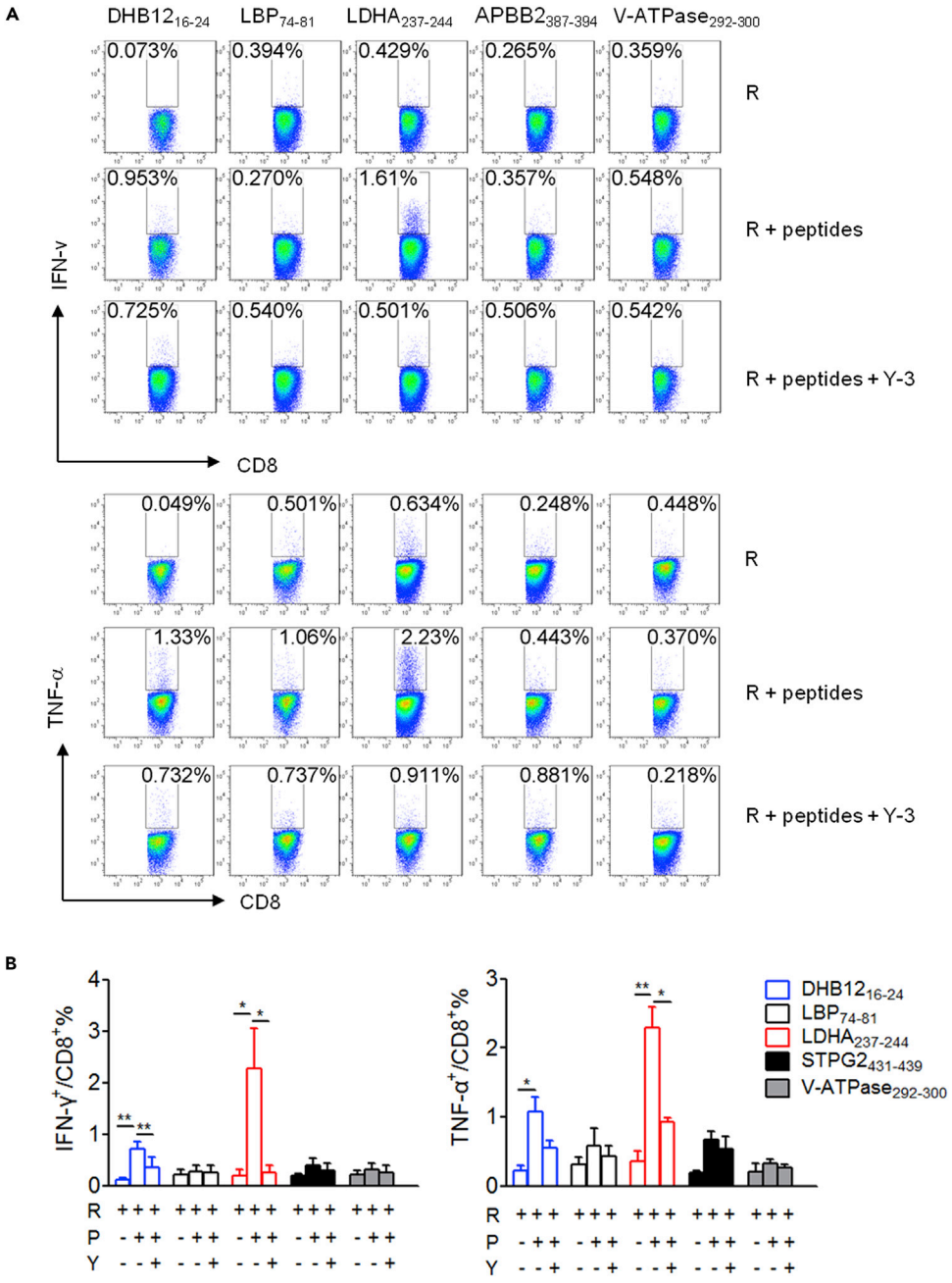

Figure 4. Immunogenicity Characterization of Single Peptide in Group 1

(A) Representative FACS plots depicting intracellular IFN-γ and TNF-α staining of $CD8^+$ T cells restimulated with RMAS cells (R) alone, or R loaded with the indicated peptide, or in the presence of Y-3 antibody.

(B) Summary graph for FACS analysis in (A). Each bar represents the mean ± SEM of three independent experiments. *$p < 0.05$; **$p < 0.01$ determined by Student's t test.

See also Figure S3 and Table S6.

a peptide derived from lactate dehydrogenase (LDH) A or B chain, named $LDHA_{237-244}$, induced a strong peptide-specific $CD8^+$ T cell pro-inflammatory response. Similarly, Y-3 almost eliminated the $CD8^+$ T cell response primed by these two peptides. The other peptides did not prime any apparent $CD8^+$ T cell response (Figures 4A and 4B). As negative controls, $CATA_{384-392}$ and $PLIN2_{213-221}$ in G3 remained non-immunogenic (Figures S3A and S3B). These data indicate that HFD-induced obesity results in generation of exclusive immunogenic peptides in obese VAT for driving $CD8^+$ T cell pro-inflammatory responses.

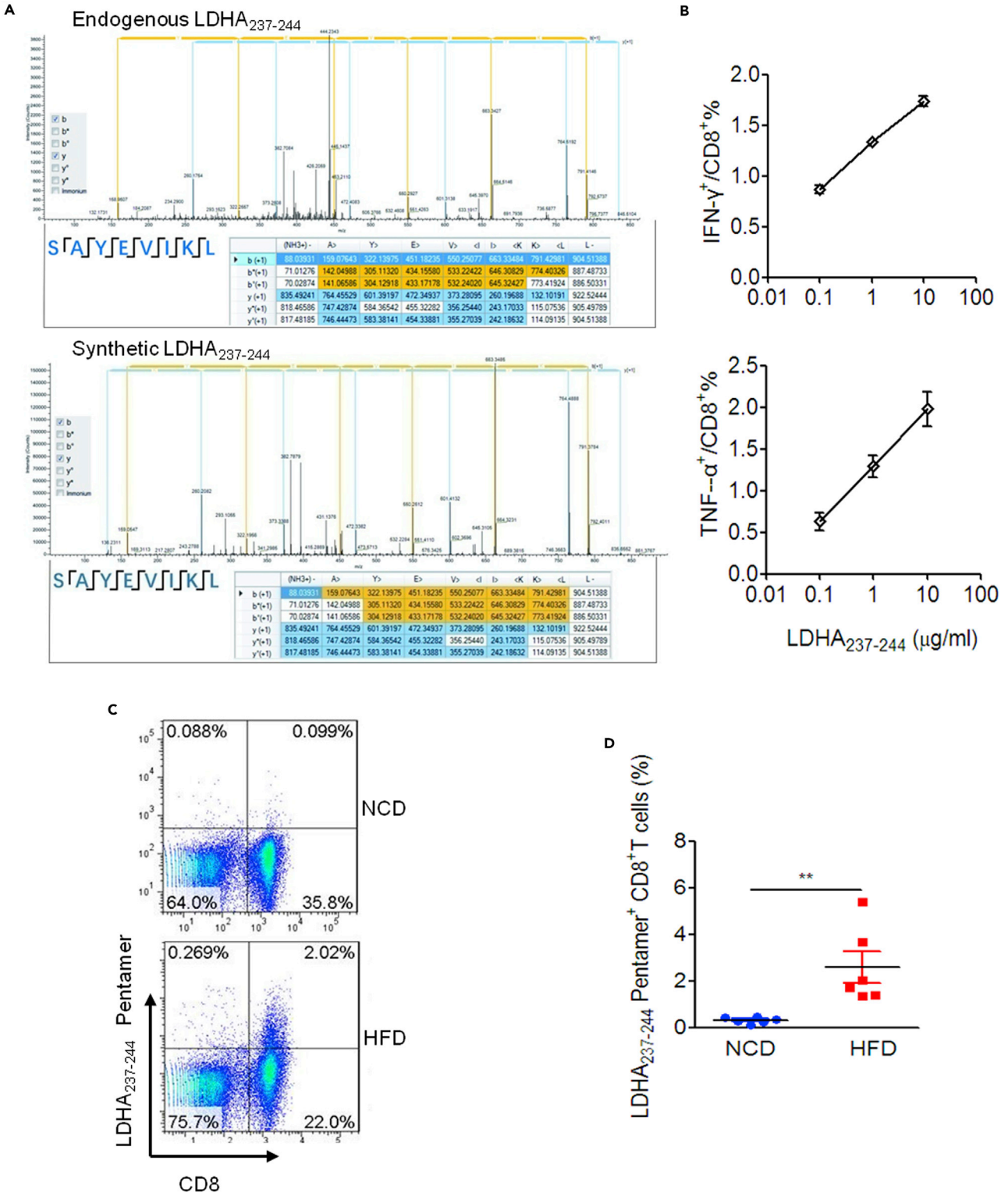

Figure 5. Peripheral CD8$^+$ T Cells Recognize LDHA$_{237-244}$ Peptide in HFD-Induced Obese Mice

(A) Tandem mass spectra of endogenous LDHA$_{237-244}$ (upper: m/z 461.76538Da) and its corresponding synthetic peptide (lower: m/z 461.76566Da).

(B) Statistical graph of the frequency of IFN-γ- and TNF-α-producing cells among the CD8$^+$ T cells primed by various concentrations of LDHA$_{237-244}$ peptide.

Figure 5. *Continued*

(C) Exemplified FACS plots of the lymphocytes from the mesenteric lymph nodes of HFD-fed (obese) mice and NCD-fed (lean) mice stained with H2-Kb/$LDHA_{237-244}$ pentamer (Proimmune) and anti-mouse CD8 antibody.

(D) Summary graph of FACS analysis of the frequency of H2-Kb/$LDHA_{237-244}$ pentamer positive $CD8^+$ T cells in the mesenteric lymph nodes from NCD and HFD-fed mice after 8-week HFD or NCD administration (n = 6 per group). The results are representative of one of two independent experiments. Data are presented as scatterplots with minimum and maximum values for data distribution. $^{**}p < 0.01$.

See also Figure S4.

$LDHA_{237-244}$-Specific $CD8^+$ T Cells Are Present in HFD-Induced Obese Mice

Since the $LDHA_{237-244}$ peptide is immunogenic, and exists exclusively in the MIP derived from obese VAT, we considered whether $LDHA_{237-244}$-specific $CD8^+$ T cells are associated with obesity in mice. First, in order to exclude the potential error due to mass spectrometry, we compared the secondary tandem mass spectra of identified endogenous $LDHA_{237-244}$ and its synthetic counterpart. Although there remained mild deviations between the two secondary mass spectrum that may have been induced by the difference in the fragmentation form of these two peptides during detection, we observed that the sequences identified for these two peptides were identical and the molecular weights were almost identical. This basically confirmed the accuracy of mass spectrum identification of endogenous $LDHA_{237-244}$ peptides (Figure 5A). The immunogenicity of synthetic $LDHA_{237-244}$ peptide was further verified by peptide dose-dependent stimulation of $CD8^+$ T cells to produce IFN-γ and TNF-α (Figure 5B). Next, the presence of peripheral $LDHA_{237-244}$-specific $CD8^+$ T cells in HFD-induced obese mice was confirmed by phycoerythrin (PE)-labeled H2-Kb/$LDHA_{237-244}$ pentamer staining (Figure 5C). As expected, significantly higher levels of peripheral H2-Kb/$LDHA_{237-244}$ pentamer positive $CD8^+$ T cells were detected in HFD-induced obese mice as compared with lean control mice (Figure 5D). To further confirm the presence of $LDHA_{237-244}$ peptide-reactive Th1-like $CD8^+$ T cells in VAT from obese mice, we stimulated VAT-infiltrated lymphocytes collected from obese mice and lean mice with RMAS cells loaded with or without $LDHA_{237-244}$ peptide, respectively, and determined the intracellular IFN-γ secretion in VAT $CD8^+$ T cells. Although the $LDHA_{237-244}$ peptide-pulsed RMAS cells significantly stimulated the secretion of IFN-γ by VAT-infiltrated $CD8^+$ T cells in HFD-fed obese mice, the same was not observed in lean mice (Figures S4A). These data indicated that the $LDHA_{237-244}$ peptide represents an obesity-associated target recognized by peripheral and VAT-infiltrated $CD8^+$ T cells in HFD-induced obese mice. Therefore, we wanted to investigate whether HFD-induced obesity and metabolic disorders can be alleviated by induction of $LDHA_{237-244}$ peptide-specific $CD8^+$ T cell tolerance. Unfortunately, both intranasal and intraperitoneal administration of a single $LDHA_{237-244}$ peptide repeatedly failed to affect weight gain, glucose intolerance, and insulin resistance in HFD-fed mice significantly (Figures S4B and S4C).

Source Proteins of $LDHA_{237-244}$ Peptide Are Downregulated in Obese Mice

MHC class I-associated peptides are derived from source proteins degraded through the ubiquitin-proteasome pathway. There are two types of proteasomes, constitutive proteasome and immunoproteasome, responsible for generating peptides presented by MHC class I molecules. The immunoproteasome is believed to elicit greater competence at producing immunodominant peptides. We observed that the mRNA levels of constitutive proteasome, particularly that of immunoproteasome catalytic subunit genes, were significantly higher in obese VAT than in lean VAT (Figure S5), suggesting a hyperactive antigen processing machinery in obesity. Furthermore, we wanted to investigate whether the H2-Kb-presented $LDHA_{237-244}$ peptide is generated in obese VAT due to the altered expression of its source proteins. In general, higher gene expression can favor peptide presentation. However, we observed that the mRNA expression of both *Ldha* and *Ldhb* did not alter significantly between NCD VAT and HFD VAT (data not shown). On the contrary, our mass spectrometry analysis of VAT proteome indicated that both LDHA and LDHB protein levels in obese VAT were significantly lower when compared with that in lean VAT (Figure 6A). We observed that LDHA expression was dominant in VAT (Figure 6A); western blotting analysis confirmed that the LDHA protein levels were significantly lower in obese VAT (Figure 6B). Consistent with these results, the enzyme activity of LDH in obese VAT decreased significantly when compared with that in lean VAT (Figure 6C). However, the LDH enzyme activity in skeletal muscle tissue did not differ between lean and obese mice (data not shown). Therefore, these results indicate that LDHA/LDHB stability might decrease in obese VAT. Since Lys48-linked ubiquitins act as a universal signal for proteins targeted for proteosomal degradation, we further investigated whether LDHA underwent increased Lys48-linked ubiquitination in obese VAT and whether proteasome was involved in the degradation of Lys48-ubiquitinated LDHA in VAT. Total protein was extracted from HFD VAT and NCD VAT in the presence or absence of MG132 (a proteasome inhibitor), after which protein extract was immunoprecipitated using anti-LDHA

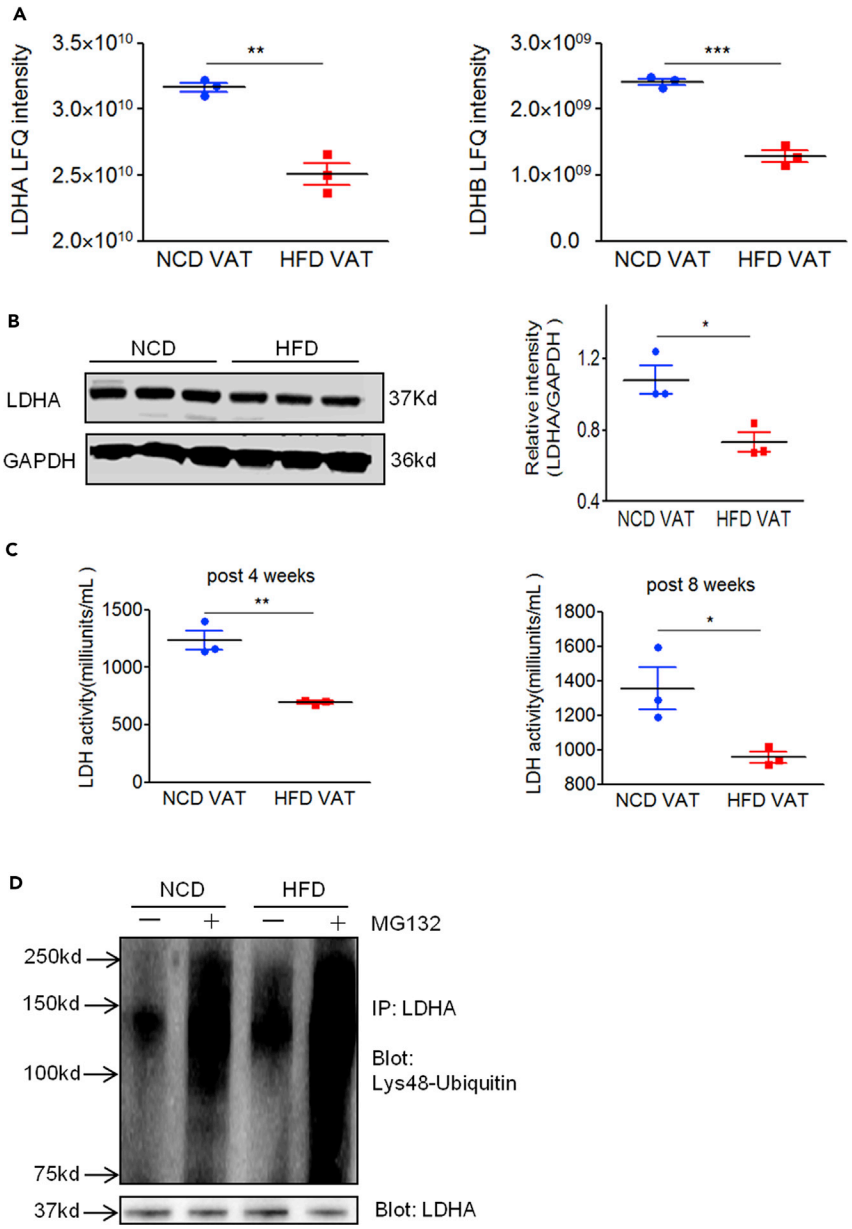

Figure 6. The Source Proteins of LDHA237-244 Peptide Are Downregulated in Obese Mice

(A) Comparison of LDHA and LDHB peptide levels in NCD VAT and HFD VAT samples measured by LFQ ion intensities revealed a significant decrease in both LDHA and LDHB peptide levels in obese VAT. Error bars represent ±SD (each data point consists of VAT samples pooled from 3–4 mice).

(B) Quantitative western blot analysis of LDHA in VAT of C57BL/6 mice administered NCD or HFD for 4 weeks (n = 3 per group). Error bars represent ±SD.

(C) Summary graph of the LDH activity levels in VAT isolated from C57BL/6 mice administered NCD or HFD for 4 and 8 weeks (n = 3 per group) determined using an LDH activity assay kit. The results are representative of one of two independent experiments. Error bars represent ±SD.

(D) The epididymal fat pads (VAT samples) were collected from three or four obese or lean mice fed with HFD or NCD for 8 weeks, respectively, and total protein was extracted from HFD or NCD VAT in the presence or absence of MG132 (10 μM). The VAT protein solution was immunoprecipitated with anti-LDHA antibodies. Eluted proteins were subjected to western blot analysis and probed with specific antibodies against Lys48-specific ubiquitin and LDHA. Data are representative of two experiments. *$p < 0.05$; **$p < 0.01$; ***$p<0.001$, determined by Student's t test.

See also Figure S5.

antibodies. Immunoblotting using anti-Lys48-linked ubiquitin antibody revealed that the basal level of Lys48-linked ubiquitination of LDHA in HFD VAT was higher than that in NCD VAT. Moreover, inhibition of the proteasome by MG132 markedly enhanced the accumulation of Lys48-linked ubiquitinated LDHA in VAT (Figure 6D). Considered in conjunction, we inferred that the generation of H2-Kb-restricted $LDHA_{237-244}$ peptide might be attributed to abnormal ubiquitin-proteasome degradation of LDHA/LDHB in obese VAT.

DISCUSSION

Obesity-induced VAT chronic inflammation is currently considered to play a pivotal role in the progression of obesity-related clinical comorbidities, such as insulin resistance, T2DM, atherosclerosis, neurodegenerative disorders, and some forms of cancer. The involvement of $CD8^+$ T cells in the initiation and propagation of obesity-related VAT chronic inflammation has been reported previously (Nishimura et al., 2009), and several studies suggest that the activation and proliferation of $CD8^+$ T cells in obese VAT may be driven by specific antigens enriched in obese VAT (Feuerer et al., 2009; Nishimura et al., 2009; Winer et al., 2009; Yang et al., 2010). However, the antigenic mechanisms driving $CD8^+$ T cell pro-inflammatory responses in obese VAT remain unknown. We adopted a large-scale mass spectrometry approach and presented an in-depth analysis of VAT-derived MIPs, comparing obese and non-obese states. We observed that HFD-induced obesity led to significant alteration in the VAT MIP landscape and obese VAT presents a unique set of MIP source proteins. Additionally, we demonstrated that some obesity-exclusive MHC class I-presented antigenic peptides were immunogenic and might contribute to the pro-inflammatory $CD8^+$ T cell responses.

When compared with the analysis of MIPs derived from cells, analysis of MIPs derived from mouse primary tissue is reported with limited success, considering the high number of mice needed to perform an experiment (Caron et al., 2015). Recently, MIPs from 19 normal tissue samples from C57BL/6 mice, excluding adipose tissue, were investigated, and the number of peptides identified in different primary tissues ranged from over hundred to thousands (Schuster et al., 2018). Considering the MIP variation in primary tissue between mice within the same treatment group and the sufficient coverage and depth of MIP identified by LC/MS, we pooled VAT samples from a large number of lean mice or obese mice from three different batches to isolate MIP for one experiment. To establish VAT MIP datasets, we performed technical triplicates for the analysis of each MIP sample and combined all high confidence peptides identified by three repeated Mascot and Sequest searches of each MIP sample. This may help in increasing the coverage and depth of identified peptides, as well as in reducing sampling errors in the comparison of different biological replicates. Although lean VAT and obese VAT expressed similar levels of H2-Kb protein, and comparable quantity of H2-Kb proteins was immunoaffinity-purified from the two samples, the number of H2-Kb-associated peptides identified in HFD VAT was close to half of the number of peptides identified in NCD VAT. We inferred that HFD VAT MIP might comprise more unconventional peptides (e.g., spliced peptides) that cannot be identified in a conventional database search.

MIP is not a reflection of the proteome and presents a small fraction of the proteome (Pearson et al., 2016). Comprehensive analysis of MIP is significant for identification of novel antigenic targets and potential biomarker signatures in diseases. It has been reported that the defined unique tumor MIP reflects tumor-associated pathways implicated in oncogenesis and complex alterations in tumor cell metabolism result in non-mutated tumor-specific antigenic targets for immunotherapeutic applications (Loffler et al., 2018). By comparing the two MIP datasets, we observed that HFD-induced obesity significantly altered the VAT MIP landscape. We screened out HFD VAT-exclusive peptides at the source protein level and observed that HFD VAT-exclusive MIP source proteome conceals a distinct obesity-associated signature. The KEGG pathway enrichment analysis revealed that the HFD VAT-exclusive MIP source protein content was significantly enriched in some pathways, such as aldosterone synthesis and secretion (Dinh Cat et al., 2016), glucagon signaling (Charron and Vuguin, 2015), calcium signaling (Bravo-Sagua et al., 2017), cGMP-PKG signaling (Kovacs et al., 2016), propanoate metabolism (Chen et al., 2015), and cAMP signaling pathway (Madsen and Kristiansen, 2010), and abnormalities in these pathways are closely associated with obesity-related metabolic diseases. Notably, previously identified obesity-related proteins or biomarkers, such as LBP (Kim et al., 2016), GPR50 (Ivanova et al., 2008), PLTP (Qin et al., 2014) (Tzotzas et al., 2009), and mitochondrial glycerol 3-phosphate dehydrogenase (Zheng et al., 2019), were detected as obese VAT-exclusive MIP source proteins (Table S2). We proposed that these proteins are likely to be expressed or modified abnormally and, hence, degraded into peptides and enter the MHC class I

presentation pathway in obese VAT. Therefore, discovery of MIP source proteins using large-scale analyses might represent a feasible strategy to detect the key molecular targets involved in pathogenesis for diagnosis and prevention of obesity and its related metabolic disorders.

In this study, we hypothesized that certain MHC class I-presented antigenic peptides derived exclusively from aberrant proteins on overloaded adipocytes might be recognized specifically by $CD8^+$ T cells that initiate obesity-induced inflammation. As expected, certain MHC I-restricted peptides, such as $LDHA_{237-244}$, present exclusively in obese VAT MIPs and undetectable in normal VAT MIPs, exhibited dose-dependent immunogenicity to induce $CD8^+$ T cell responses. Furthermore, we demonstrated that the $LDHA_{237-244}$-specific $CD8^+$ T cells were present in obese mice, whereas they were absent in lean mice. The results suggested that the alterations in VAT MIP landscape in obesity may be accompanied by the generation of obesity-exclusive antigenic peptides that might not be presented at the T cell negative selection stage or at the steady state and, thus, are immunogenic for $CD8^+$ T cell activation and consequent initiation of adipose tissue inflammation. Therefore, these obesity-exclusive antigenic peptides may be potential targets for the prevention of obesity-related chronic inflammation. However, we observed that repeated intranasal or intraperitoneal administration of a single $LDHA_{237-244}$ peptide failed to affect HFD-induced obesity and abnormal glucose metabolism significantly. This failure might be attributed to the existence of multiple antigenic peptides in obese VAT that are responsible for triggering and maintaining multiantigen-specific $CD8^+$ T cell-mediated chronic inflammatory response in obese VAT. Therefore, different obese VAT-relevant antigens/peptides need to be identified in future. The early activation and amplification of tissue-resident $CD8^+$ T cells is reportedly involved in the progression of other inflammatory diseases, such as hypertension-related cardiovascular inflammation (Ma et al., 2014) and non-alcoholic fatty liver disease (Ghazarian et al., 2017; Wolf et al., 2014). Considering that MHC class I molecules are widely expressed in nucleated somatic cells, we hypothesized that the functions of $CD8^+$ T cells are not just limited to monitoring of infected host cells or malignant transformed cells; it extends to monitoring of abnormal host cells in which MHC I molecules present "abnormal-antigenic peptides" under certain pathological conditions as well, thus initiating early inflammation or cascading autoimmune responses. Additional evidence is necessary to support this perspective.

The MIP repertoire originates primarily from ubiquitin-proteasome-dependent degradation of source proteins that include miscoded/misfolded or mismodified proteins, premature translation-termination products, intrinsically disordered proteins, and some regulatory proteins among others that temporarily regulate the cellular activities (de Verteuil et al., 2012; Sijts and Kloetzel, 2011). The MIPs generated by the constitutive proteasome and the immunoproteasome are proposed to differ quantitatively and qualitatively (Van den Eynde and Morel, 2001). We suggest that the obese VAT MIP landscape differs significantly from that of lean fat MIP, partly due to significant upregulation of immunoproteasome in obese VAT. The constitutive proteasome contains three catalytic subunits, namely, β1 (PSMB1), β2 (PSMB1), and β5, and plays a critical role in structuring MHC class I-presenting self-peptide under steady conditions in non-lymphoid tissues. The immunoproteasome, including LMP2 (PSMB8), LMP7 (PSMB9), and MECL1 (PSMB10), is constitutively expressed by mature dendritic cells and upregulated when cells are stimulated by inflammatory stimuli. Studies on tumor immunology have reported production of tumor antigenic peptides by the immunoproteasome and the intermediate conformations, whereas the same was not reported for constitutive proteasome (Vigneron and Van den Eynde, 2014). It has been reported that an immunoproteasome subunit LMP7 deficiency in both immune cells and non-immune cells attenuated adipose tissue inflammation and prevented the development of obesity and metabolic disorders (Kimura et al., 2015), providing further support to our perspective on the probable involvement of immunoproteasomes in generation of obesity-associated antigenic peptides for priming pro-inflammatory $CD8^+$ T cell responses.

Lys48-linked polyubiquitin molecules are key regulators of protein degradation mediated by the proteasome (Wilkinson et al., 1995). We observed that the protein levels of the candidate source proteins of $LDHA_{237-244}$ peptide, LDHA/LDHB, were reduced in obese VAT; moreover, the Lys48-linked ubiquitination of LDHA was upregulated in obese VAT compared with lean VAT, and inhibition of the proteasome markedly enhanced the accumulation of Lys48-linked ubiquitinated LDHA in VAT, suggesting an increased ubiquitin-proteasome degradation and MHC class I-associated presentation of LDHA or LDHB occurring in obese VAT. The LDHA or LDHB subunit can assemble into homo- or hetero-tetramers that catalyze the interconversion of pyruvate and lactate with concomitant interconversion of NADH and NAD^+ to maintain normal metabolic flux. However, the limited studies on the correlation between LDH in

VAT and obesity remain controversial so far. Selected studies have demonstrated that obese individuals exhibit high LDH activity in correlation with high lactate accumulation in multiple tissues (Jha and Mitra Mazumder, 2019; Piantedosi et al., 2016). Conversely, LDHA was reported to be downregulated in obese adipose tissue, resulting in the direction of pyruvate into acetyl-CoA production, which in turn promotes fatty acid biosynthesis and triglyceride storage (Lopez et al., 2004). Given lactate has been indicated to induce browning of white adipose cells in mice and humans by enhancing thermogenic gene expression (Carriere et al., 2014), it has been suggested that increasing the LDHA protein levels in adipose tissue might prevent obesity, which in turn would increase conversion of pyruvate to lactate (Parray and Yun, 2015). Our results suggest that the stability of LDHA in obese VAT is reduced due to its excessive ubiquitin-proteasome degradation, which may further disrupt metabolic flux and promote obesity. The exact role of VAT LDH in obesity-related metabolic diseases and the underlying mechanisms need to be investigated extensively.

To summarize, this study confirmed the molecular composition of obese VAT MIP determined by high-throughput and high-resolution MS, reflecting a distinctive obesity-associated signature that is affected by the metabolic status of adipocytes. The obese VAT-exclusive antigenic peptides generated from abnormal protein degradation may function as the antigenic factors that drive the pro-inflammatory responses of $CD8^+$ T cells in VAT, representing a mechanism underlying obesity-induced VAT inflammation. Identification of obesity-exclusive adipose tissue antigenic targets should pave the way for the development of antigen-specific strategies for prevention of obesity-related chronic VAT inflammation and its related diseases.

Limitations of the Study

One of the major limitations of our study was the lack of biological replicates for VAT-derived MIP identification, which is more helpful in demonstrating HFD VAT specificity of certain peptides definitively. The current limitations of mass spectrometry analysis and database search strategies for MIP make it difficult to identify extremely low-abundance peptides and unconventional peptides in the present study. Although adipocytes are the primary components of adipose tissue, we cannot completely rule out the contribution of obesity-related immunogenicity peptides from other stromal cells in adipose tissue. Utilization of normal or hypertrophic mature adipocytes differentiated from 3T3-L1 for MIP analysis is a topic worthy of further study.

METHODS

All methods can be found in the accompanying Transparent Methods supplemental file.

DATA AND CODE AVAILABILITY

Raw mass spectrometry files are available at http://www.immunoinformatics.net/upload/MS/. The mzXML format of raw mass spectrometry files converted by msConvert (Chambers et al., 2012) are provided as well.

SUPPLEMENTAL INFORMATION

Supplemental Information can be found online at https://doi.org/10.1016/j.isci.2020.100977.

ACKNOWLEDGMENTS

This work was supported by the National Key Project for Research & Development of China (Grant no. 2016YFA0502204) and the National Natural Science Foundation of China (No. 81273213, No. 31570931, and No. 81871301).

AUTHOR CONTRIBUTIONS

X.C. and S.W. performed *ex vivo*, *in vitro*, and *in vivo* experiments, analyzed data, and wrote the manuscript. Y.H. and S.W. performed the mass spectrometry experiments and analyzed the MIP data. X.Z. conducted bioinformatics analysis. X.J. and G.M. supported *in vitro* functional analyses of peptide-specific T cell response. Q.Z. and M.J. performed *in vitro* qPCR and WB analyses of adipose tissue. Y.W. contributed substantially to the conceptualization and discussion of the project and contributed to writing of the manuscript. L.W. conceptualized and designed the study, analyzed and interpreted data, and wrote the manuscript.

DECLARATION OF INTERESTS

The authors declare no competing interests.

Received: September 26, 2019
Revised: January 21, 2020
Accepted: March 9, 2020
Published: April 24, 2020

REFERENCES

Adamopoulou, E., Tenzer, S., Hillen, N., Klug, P., Rota, I.A., Tietz, S., Gebhardt, M., Stevanovic, S., Schild, H., Tolosa, E., et al. (2013). Exploring the MHC-peptide matrix of central tolerance in the human thymus. Nat. Commun. *4*, 2039.

Bassani-Sternberg, M., Braunlein, E., Klar, R., Engleitner, T., Sinitcyn, P., Audehm, S., Straub, M., Weber, J., Slotta-Huspenina, J., Specht, K., et al. (2016). Direct identification of clinically relevant neoepitopes presented on native human melanoma tissue by mass spectrometry. Nat. Commun. *7*, 13404.

Boon, T., Coulie, P.G., Van den Eynde, B.J., and van der Bruggen, P. (2006). Human T cell responses against melanoma. Annu. Rev. Immunol. *24*, 175–208.

Bravo-Sagua, R., Parra, V., Lopez-Crisosto, C., Diaz, P., Quest, A.F., and Lavandero, S. (2017). Calcium transport and signaling in mitochondria. Compr. Physiol. *7*, 623–634.

Caron, E., Kowalewski, D.J., Chiek Koh, C., Sturm, T., Schuster, H., and Aebersold, R. (2015). Analysis of major histocompatibility complex (MHC) immunopeptidomes using mass spectrometry. Mol. Cell. Proteomics *14*, 3105–3117.

Caron, E., Vincent, K., Fortier, M.H., Laverdure, J.P., Bramoulle, A., Hardy, M.P., Voisin, G., Roux, P.P., Lemieux, S., Thibault, P., et al. (2011). The MHC I immunopeptidome conveys to the cell surface an integrative view of cellular regulation. Mol. Syst. Biol. *7*, 533.

Carriere, A., Jeanson, Y., Berger-Muller, S., Andre, M., Chenouard, V., Arnaud, E., Barreau, C., Walther, R., Galinier, A., Wdziekonski, B., et al. (2014). Browning of white adipose cells by intermediate metabolites: an adaptive mechanism to alleviate redox pressure. Diabetes *63*, 3253–3265.

Chambers, M.C., Maclean, B., Burke, R., Amodei, D., Ruderman, D.L., Neumann, S., Gatto, L., Fischer, B., Pratt, B., Egertson, J., et al. (2012). A cross-platform toolkit for mass spectrometry and proteomics. Nat. Biotechnol. *30*, 918–920.

Charron, M.J., and Vuguin, P.M. (2015). Lack of glucagon receptor signaling and its implications beyond glucose homeostasis. J. Endocrinol. *224*, R123–R130.

Chen, H.H., Tseng, Y.J., Wang, S.Y., Tsai, Y.S., Chang, C.S., Kuo, T.C., Yao, W.J., Shieh, C.C., Wu, C.H., and Kuo, P.H. (2015). The metabolome profiling and pathway analysis in metabolic healthy and abnormal obesity. Int. J. Obes. (Lond.) *39*, 1241–1248.

de Verteuil, D., Granados, D.P., Thibault, P., and Perreault, C. (2012). Origin and plasticity of MHC I-associated self peptides. Autoimmun. Rev. *11*, 627–635.

de Verteuil, D., Muratore-Schroeder, T.L., Granados, D.P., Fortier, M.H., Hardy, M.P., Bramoulle, A., Caron, E., Vincent, K., Mader, S., Lemieux, S., et al. (2010). Deletion of immunoproteasome subunits imprints on the transcriptome and has a broad impact on peptides presented by major histocompatibility complex I molecules. Mol. Cell Proteomics *9*, 2034–2047.

Dinh Cat, A.N., Friederich-Persson, M., White, A., and Touyz, R.M. (2016). Adipocytes, aldosterone and obesity-related hypertension. J. Mol. Endocrinol. *57*, F7–F21.

Dutoit, V., Herold-Mende, C., Hilf, N., Schoor, O., Beckhove, P., Bucher, J., Dorsch, K., Flohr, S., Fritsche, J., Lewandrowski, P., et al. (2012). Exploiting the glioblastoma peptidome to discover novel tumour-associated antigens for immunotherapy. Brain *135*, 1042–1054.

Feuerer, M., Herrero, L., Cipolletta, D., Naaz, A., Wong, J., Nayer, A., Lee, J., Goldfine, A.B., Benoist, C., Shoelson, S., et al. (2009). Lean, but not obese, fat is enriched for a unique population of regulatory T cells that affect metabolic parameters. Nat. Med. *15*, 930–939.

Ghazarian, M., Revelo, X.S., Nohr, M.K., Luck, H., Zeng, K., Lei, H., Tsai, S., Schroer, S.A., Park, Y.J., Chng, M.H.Y., et al. (2017). Type I interferon responses drive intrahepatic T cells to promote metabolic syndrome. Sci. Immunol. *2*, https://doi.org/10.1126/sciimmunol.aai7616.

Gonzalez-Duque, S., Azoury, M.E., Colli, M.L., Afonso, G., Turatsinze, J.V., Nigi, L., Lalanne, A.I., Sebastiani, G., Carre, A., Pinto, S., et al. (2018). Conventional and neo-antigenic peptides presented by beta cells are targeted by circulating naive CD8+ T cells in type 1 diabetic and healthy donors. Cell Metab. *28*, 946–960.e6.

Granados, D.P., Laumont, C.M., Thibault, P., and Perreault, C. (2015). The nature of self for T cells-a systems-level perspective. Curr. Opin. Immunol. *34*, 1–8.

Ivanova, E.A., Bechtold, D.A., Dupre, S.M., Brennand, J., Barrett, P., Luckman, S.M., and Loudon, A.S. (2008). Altered metabolism in the melatonin-related receptor (GPR50) knockout mouse. Am. J. Physiol. Endocrinol. Metab. *294*, E176–E182.

Jha, D., and Mitra Mazumder, P. (2019). High fat diet administration leads to the mitochondrial dysfunction and selectively alters the expression of class 1 GLUT protein in mice. Mol. Biol. Rep. *46*, 1727–1736.

Kim, K.E., Cho, Y.S., Baek, K.S., Li, L., Baek, K.H., Kim, J.H., Kim, H.S., and Sheen, Y.H. (2016). Lipopolysaccharide-binding protein plasma levels as a biomarker of obesity-related insulin resistance in adolescents. Korean J. Pediatr. *59*, 231–238.

Kimura, H., Usui, F., Karasawa, T., Kawashima, A., Shirasuna, K., Inoue, Y., Komada, T., Kobayashi, M., Mizushina, Y., Kasahara, T., et al. (2015). Immunoproteasome subunit LMP7 deficiency improves obesity and metabolic disorders. Sci. Rep. *5*, 15883.

Kovacs, A., Alogna, A., Post, H., and Hamdani, N. (2016). Is enhancing cGMP-PKG signalling a promising therapeutic target for heart failure with preserved ejection fraction? Neth. Heart J. *24*, 268–274.

Kowalewski, D.J., Schuster, H., Backert, L., Berlin, C., Kahn, S., Kanz, L., Salih, H.R., Rammensee, H.G., Stevanovic, S., and Stickel, J.S. (2015). HLA ligandome analysis identifies the underlying specificities of spontaneous antileukemia immune responses in chronic lymphocytic leukemia (CLL). Proc. Natl. Acad. Sci. U S A *112*, E166–E175.

Loffler, M.W., Kowalewski, D.J., Backert, L., Bernhardt, J., Adam, P., Schuster, H., Dengler, F., Backes, D., Kopp, H.G., Beckert, S., et al. (2018). Mapping the HLA ligandome of colorectal cancer reveals an imprint of malignant cell transformation. Cancer Res. *78*, 4627–4641.

Lopez, I.P., Milagro, F.I., Marti, A., Moreno-Aliaga, M.J., Martinez, J.A., and De Miguel, C. (2004). Gene expression changes in rat white adipose tissue after a high-fat diet determined by differential display. Biochem. Biophys. Res. Commun. *318*, 234–239.

Ma, F., Feng, J., Zhang, C., Li, Y., Qi, G., Li, H., Wu, Y., Fu, Y., Zhao, Y., Chen, H., et al. (2014). The requirement of CD8+ T cells to initiate and augment acute cardiac inflammatory response to high blood pressure. J. Immunol. *192*, 3365–3373.

Madsen, L., and Kristiansen, K. (2010). The importance of dietary modulation of cAMP and insulin signaling in adipose tissue and the development of obesity. Ann. N. Y Acad. Sci. *1190*, 1–14.

McDonnell, W.J., Koethe, J.R., Mallal, S.A., Pilkinton, M.A., Kirabo, A., Ameka, M.K., Cottam, M.A., Hasty, A.H., and Kennedy, A.J. (2018). High CD8 T-cell receptor clonality and altered CDR3 properties are associated with elevated isolevuglandins in adipose tissue during diet-induced obesity. Diabetes *67*, 2361–2376.

Nishimura, S., Manabe, I., Nagasaki, M., Eto, K., Yamashita, H., Ohsugi, M., Otsu, M., Hara, K.,

Ueki, K., Sugiura, S., et al. (2009). CD8+ effector T cells contribute to macrophage recruitment and adipose tissue inflammation in obesity. Nat. Med. *15*, 914–920.

Parray, H.A., and Yun, J.W. (2015). Proteomic identification of target proteins of thiodigalactoside in white adipose tissue from diet-induced obese rats. Int. J. Mol. Sci. *16*, 14441–14463.

Pearson, H., Daouda, T., Granados, D.P., Durette, C., Bonneil, E., Courcelles, M., Rodenbrock, A., Laverdure, J.P., Cote, C., Mader, S., et al. (2016). MHC class I-associated peptides derive from selective regions of the human genome. J. Clin. Invest. *126*, 4690–4701.

Piantedosi, D., Di Loria, A., Guccione, J., De Rosa, A., Fabbri, S., Cortese, L., Carta, S., and Ciaramella, P. (2016). Serum biochemistry profile, inflammatory cytokines, adipokines and cardiovascular findings in obese dogs. Vet. J. *216*, 72–78.

Qin, S., Song, G., and Yu, Y. (2014). Phospholipid transfer protein in diabetes, metabolic syndrome and obesity. Cardiovasc. Hematol. Disord. Drug Targets *14*, 149–153.

Rausch, M.E., Weisberg, S., Vardhana, P., and Tortoriello, D.V. (2008). Obesity in C57BL/6J mice is characterized by adipose tissue hypoxia and cytotoxic T-cell infiltration. Int. J. Obes. (Lond.) *32*, 451–463.

Schuster, H., Shao, W., Weiss, T., Pedrioli, P.G.A., Roth, P., Weller, M., Campbell, D.S., Deutsch, E.W., Moritz, R.L., Planz, O., et al. (2018). A tissue-based draft map of the murine MHC class I immunopeptidome. Sci. Data *5*, 180157.

Sijts, E.J., and Kloetzel, P.M. (2011). The role of the proteasome in the generation of MHC class I ligands and immune responses. Cell Mol. Life Sci. *68*, 1491–1502.

Sun, S., Ji, Y., Kersten, S., and Qi, L. (2012). Mechanisms of inflammatory responses in obese adipose tissue. Annu. Rev. Nutr. *32*, 261–286.

Tzotzas, T., Desrumaux, C., and Lagrost, L. (2009). Plasma phospholipid transfer protein (PLTP): review of an emerging cardiometabolic risk factor. Obes. Rev. *10*, 403–411.

Van den Eynde, B.J., and Morel, S. (2001). Differential processing of class-I-restricted epitopes by the standard proteasome and the immunoproteasome. Curr. Opin. Immunol. *13*, 147–153.

Vigneron, N., and Van den Eynde, B.J. (2014). Proteasome subtypes and regulators in the processing of antigenic peptides presented by class I molecules of the major histocompatibility complex. Biomolecules *4*, 994–1025.

Wilkinson, K.D., Tashayev, V.L., O'Connor, L.B., Larsen, C.N., Kasperek, E., and Pickart, C.M. (1995). Metabolism of the polyubiquitin degradation signal: structure, mechanism, and role of isopeptidase T. Biochemistry *34*, 14535–14546.

Winer, S., Chan, Y., Paltser, G., Truong, D., Tsui, H., Bahrami, J., Dorfman, R., Wang, Y., Zielenski, J., Mastronardi, F., et al. (2009). Normalization of obesity-associated insulin resistance through immunotherapy. Nat. Med. *15*, 921–929.

Wolf, M.J., Adili, A., Piotrowitz, K., Abdullah, Z., Boege, Y., Stemmer, K., Ringelhan, M., Simonavicius, N., Egger, M., Wohlleber, D., et al. (2014). Metabolic activation of intrahepatic CD8+ T cells and NKT cells causes nonalcoholic steatohepatitis and liver cancer via cross-talk with hepatocytes. Cancer Cell *26*, 549–564.

Wu, H., Ghosh, S., Perrard, X.D., Feng, L., Garcia, G.E., Perrard, J.L., Sweeney, J.F., Peterson, L.E., Chan, L., Smith, C.W., et al. (2007). T-cell accumulation and regulated on activation, normal T cell expressed and secreted upregulation in adipose tissue in obesity. Circulation *115*, 1029–1038.

Yang, H., Youm, Y.H., Vandanmagsar, B., Ravussin, A., Gimble, J.M., Greenway, F., Stephens, J.M., Mynatt, R.L., and Dixit, V.D. (2010). Obesity increases the production of proinflammatory mediators from adipose tissue T cells and compromises TCR repertoire diversity: implications for systemic inflammation and insulin resistance. J. Immunol. *185*, 1836–1845.

Zheng, Y., Qu, H., Xiong, X., Wang, Y., Liu, X., Zhang, L., Liao, X., Liao, Q., Sun, Z., Ouyang, Q., et al. (2019). Deficiency of mitochondrial glycerol 3-phosphate dehydrogenase contributes to hepatic steatosis. Hepatology *70*, 84–97.

iScience, Volume *23*

Supplemental Information

Obesity Reshapes Visceral Fat-Derived MHC I Associated-Immunopeptidomes and Generates Antigenic Peptides to Drive $CD8^+$ T Cell Responses

Xiaoling Chen, Shufeng Wang, Yi Huang, Xia Zhao, Xu Jia, Gang Meng, Qian Zheng, Mengjun Zhang, Yuzhang Wu, and Li Wang

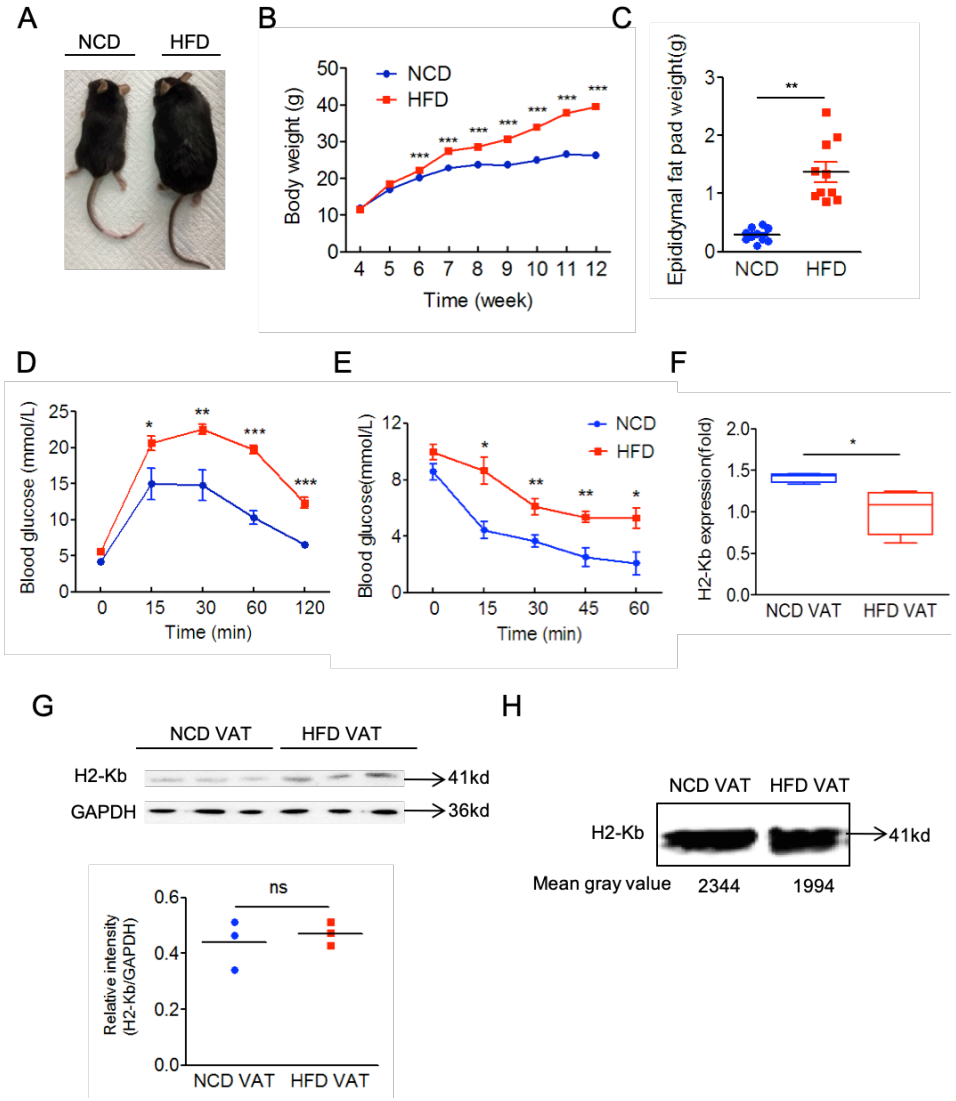

Figure S1. Establishment of high fat diet (HFD)-induced obese C57BL/6 mice model, Related to Figure 1

(A) Representative images of C57BL/6 male mice fed with a high-fat diet (HFD) or a normal diet (NCD) beginning at 4 weeks of age for 8 weeks. (B) Body weight gain of male C57BL/6 mice after 8-week HFD or NCD feeding (started at 4 weeks of age) (n=10 mice per group). The epididymal fat pad (VAT) mass from male C57BL/6 mice with HFD or NCD feeding at 12 weeks of age. (n=10 mice per group). Serum glucose levels during (D) glucose tolerance test (GTT) and (E) insulin tolerance test (ITT) in male C57BL/6 mice after 8-week HFD (n=10 mice per group). Data are means and error bars are ±SEM. Quantitative real-time PCR analysis (n=10 mice per group) (F) and immunoblotting analyses (n=3 mice per group) (G) of H2-Kb expression in the VAT of mice after 8-week HFD or NCD feeding. (H) Immunoblotting analyses of H2-Kb in Co-IP ultrafiltration superfluid from the VAT homogenates of mice after 8-week HFD or NCD feeding.

* $p < 0.05$, ** $p < 0.01$, *** $p<0.0001$, and ns: no significance, determined by Student's t-test.

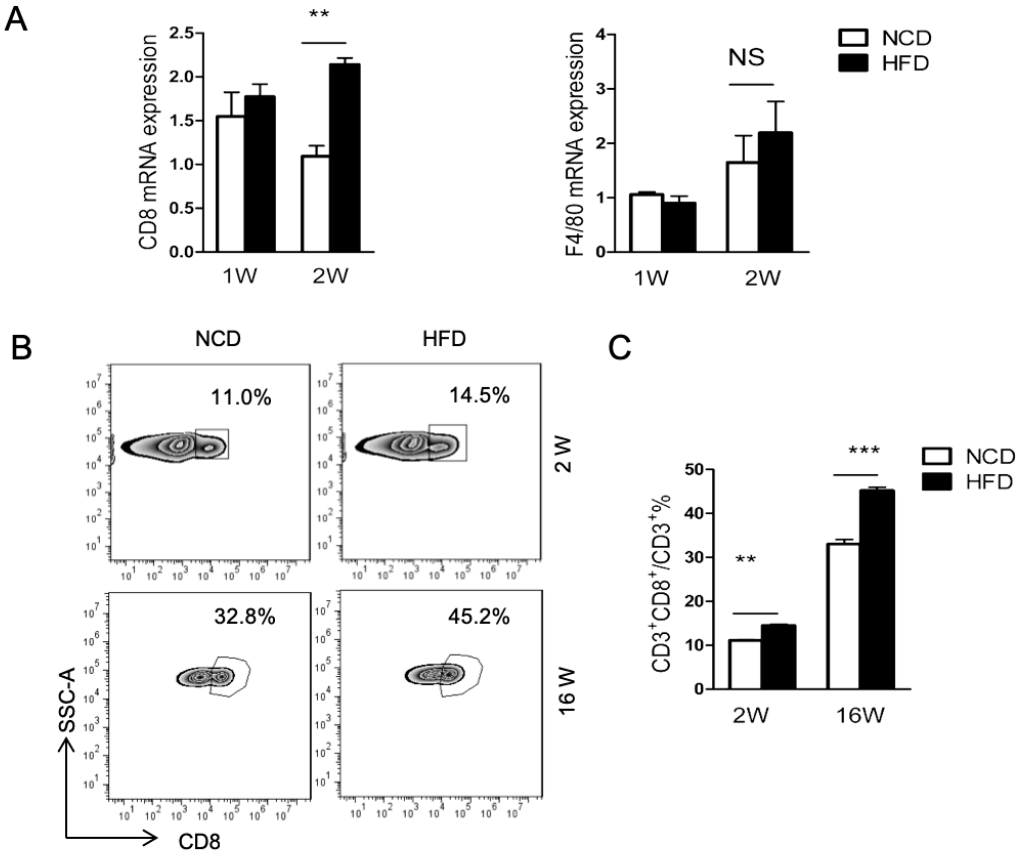

Figure S2. HFD feeding induces an early increase of $CD8^+$ T cells in visceral adipose tissues, Related to Figure 3

(A) Quantitative real-time PCR analysis of CD8 and F4/80 expression in the epididymal fat pads from mice fed with NCD and HFD for 1 or 2 weeks (started at 4 weeks of age) (n=10 mice per group). Data are means and error bars are ±SEM. Student's t test, *p < 0.05 and **p < 0.01, ***P<0.0001

(B) Representative FACS analysis of the proportion of infiltrated CD8+ T cells in the epididymal fat pads from mice fed with NCD and HFD for 2 or 16 weeks (started at 4 weeks of age). (C) Summary graph for FACS analysis of the frequency of infiltrated CD8+ T cells in the epididymal fat pads from mice fed with NCD and HFD for 2 and 16 weeks. Data are means and error bars are ±SEM.

* p < 0.05, ** p < 0.01, *** p<0.0001, and NS: no significance, determined by Student's t-test.

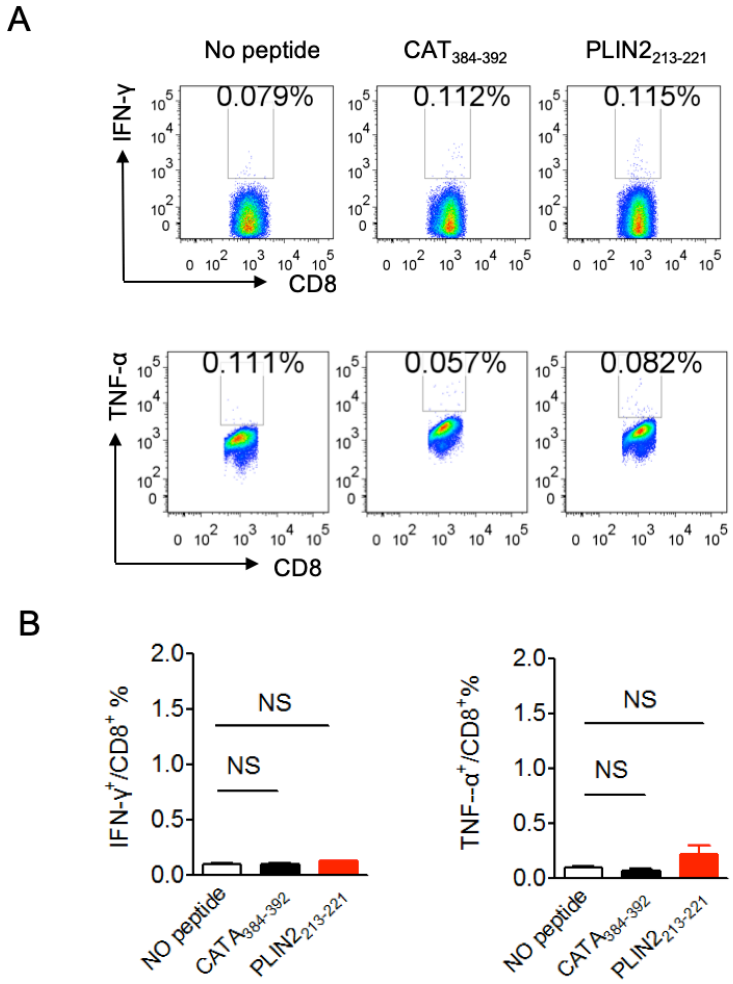

Figure S3. The peptides shared by VAT-MIPs from both NCD and HFD-fed mice have no ability to prime CD8$^+$ T cells response, Related to Figure 4

(A) Representative FACS plots indicating intracellular IFN-γ and TNF-α staining of CD8$^+$ T cells stimulated with the indicated peptides-loaded RAMS cells.

(B) Summary graph for FACS analysis of the frequency of IFN-γ and TNF-α-producing cells among CD8$^+$ T cells stimulated with the indicated peptides. Each bar represents the mean ± SEM of three independent experiments. NS: no significance, determined by Student's t-test.

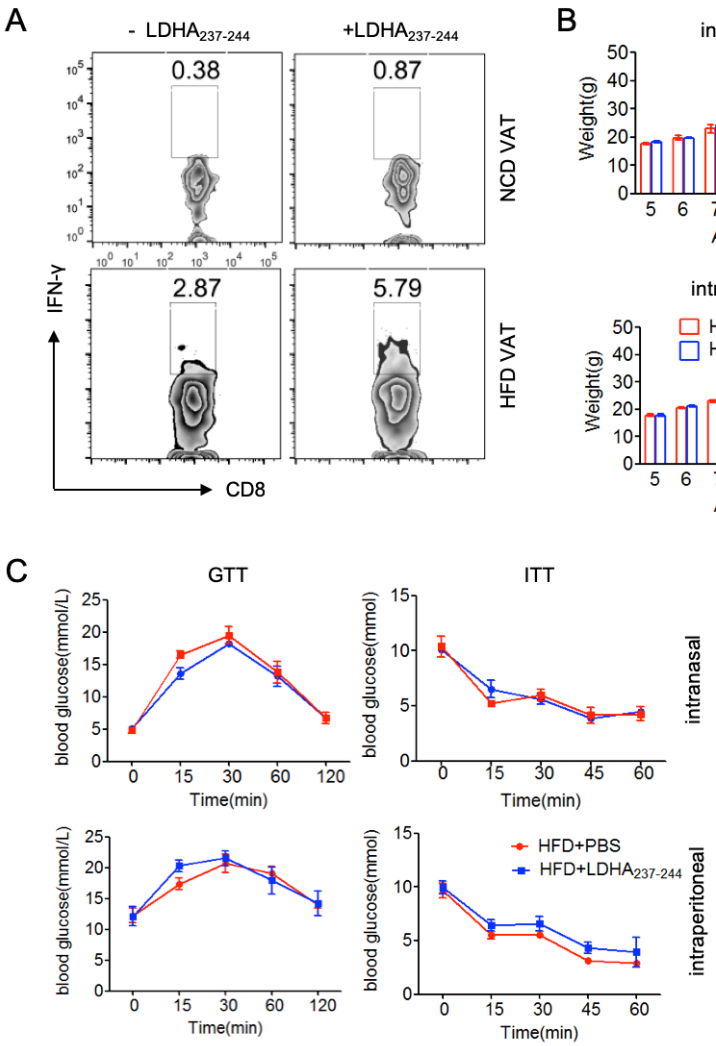

Figure S4. Intranasal or intraperitoneal administration of a single $LDHA_{237-244}$ peptide fails to affect the weight gain, glucose intolerance and insulin resistance in HFD-fed obese mice, Related to Figure 5

(A) Representative FACS indicating intracellular IFN-γ staining of VAT-infiltrated $CD8^+$ T cells stimulated with RMAS cells with RMAS cells loaded with or without $LDHA_{237-244}$ peptide.

(B) Comparison of changes in body weight between high-fat diet (HFD)-fed mice treated intranasally (upper) or intraperitoneally (lower) with $LDHA_{237-244}$ and PBS (n=4-5 mice per group). Error bars represent means ± SEM.

(C) Results of glucose tolerance (GTT) (i.p. 1 g per kg glucose, after 16 h fasting) and insulin tolerance (ITT) (i.p.,0.75 U insulin per kg body weight, after 3.5 h fasting) tests in HFD-fed mice treated intranasally (upper) or intraperitoneally (lower) with $LDHA_{237-244}$ and PBS (n =5 mice per group). Error bars represent means ± SEM. Data are representative of two experiments.

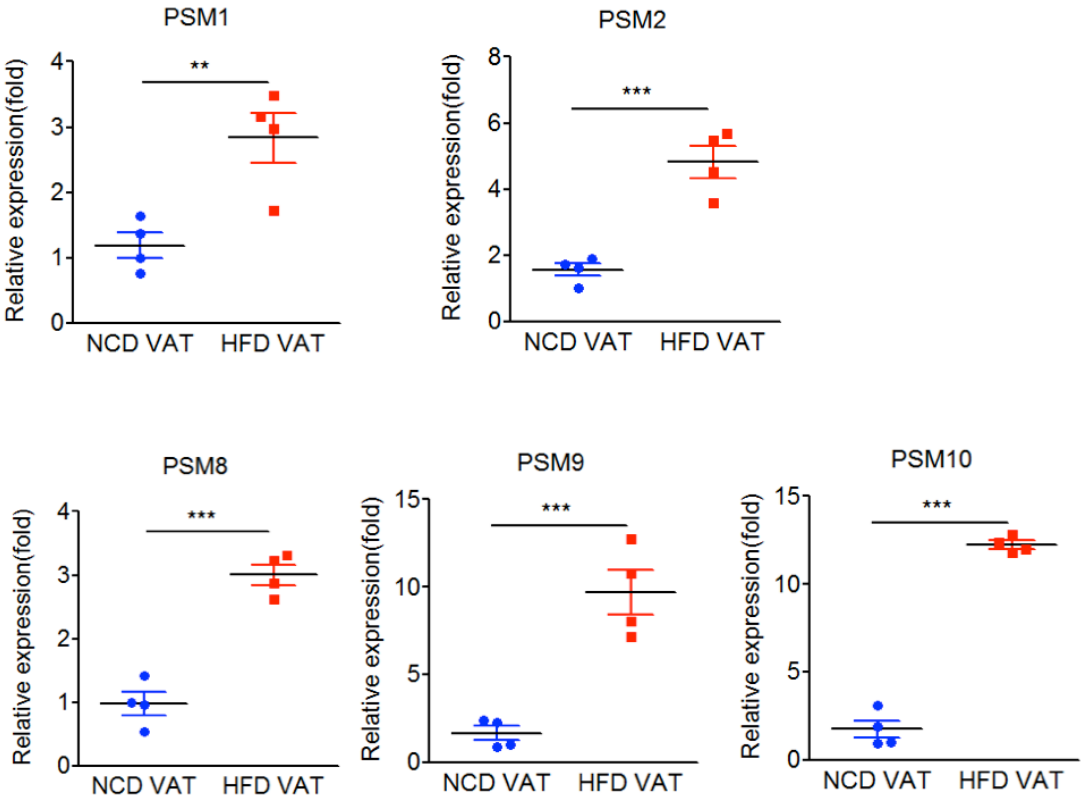

Figure S5. The mRNA expression of proteasomes (PSM1/2) and immunoproteasomes (PSM8/9/10) is increased in obese visceral adipose tissues, Related to Figure 6

Quantitative real-time PCR analysis of the mRNA expression of proteasomes (PSM1/2) and immunoproteasomes (PSM8/9/10) catalytic subunits in the epididymal fat pads from mice after 4-week NCD or HFD feeding (4 mice per group) Data are means and error bars are ±SEM.

* $p < 0.05$, ** $p < 0.01$,and *** $p<0.0001$, determined by Student's t-test.

Table S3. The exclusive high confidence H2-Kb-bound peptides from visceral adipose tissues of HFD-fed mice, Related to Figure 2

HFD VAT-exclusive MIP	Sequence	Length	Charge	MH+ [Da]	ΔM [ppm]	RT [min]	Proteins	Protein Accessions	Mascot IonScore	Sequest q-Value	MHC binding Affinity (IC_{50} nM)
1.	AALIYTSV	8	1	837.4681	-4.22	32	2	Q6PDL0,Q8R1Q8	31		67.9
2.	AAVKFHNL	8	2	899.5085	-1.48	13.39	1	Q64521	26		15.8
3.	AAYEFTTL	8	1	915.4449	-1.06	36.61	1	P32233	25		3.3
4.	ANVQYMRV	8	2	980.496	-2.34	18.99	1	Q61805	34		31.8
5.	ASTIAYLAL	9	2	922.5235	-1.04	28.57	1	O70503	28		252.5
6.	ASVVFNQL	8	2	877.477	-0.9	18.86	1	Q64288	25		10.9
7.	ATLRYASL	8	2	894.5022	-2.45	21.8	1	Q9DBR4	23		3.9
8.	DFFNYAGL	8	1	946.4321	1.68	33.05	1	P12265	27		43.4
9.	FAASYSAL	8	1	829.4089	-0.24	28.48	1	Q8BFW3	22		81.8
10.	GQYEFHSL	8	2	980.4457	-1.55	23.22	1	Q61805	33		91.9
11.	IGPYFEHNM	9	2	1107.491	-1.53	25.46	1	Q8VCB3	24		60.6
12.	ISDVRVTQL	9	2	1030.586	-3.22	31.18	1	P55065	22		355.6
13.	KSYDMSQV	8	2	957.4305	-4.36	27.95	1	Q8C8J0	21		199.4
14.	KSYLMNKL	8	2	996.5522	-2.54	17.72	3	Q01514,Q8CFB4, Q9Z0E6	28		29.4
15.	KVYTFNSV	8	2	957.5032	-0.91	21.38	3	G5E829,Q6Q477, Q9R0K7	27		10.5
16.	LAAQFSQL	8	2	877.477	-0.9	18.86	1	Q9DCB4	31		62
17.	LAPVYQRL	8	2	959.5665	-0.89	22.4	1	P82198	26		17.7
18.	NSFRYNGL	8	2	970.4738	-0.34	21.83	1	P41105	21		9.3
19.	QNYTYSSL	8	1	975.4399	-1.91	26.3	1	Q810S1	21		3.9

20.	RSYDFEFM	8	2	1094.459	-1.76	35.43	1	P40336	21		21.5
21.	SAPQFSKL	8	2	877.4777	-0.21	18.92	1	Q8K007	28		13.9
22.	SAPQYSRL	8	2	921.4781	-0.88	14.1	1	Q8CFG0	24		8.1
23.	SAYQRGESL	9	2	1010.488	-2.32	12.24	1	O35382	26		233.2
24.	SGLKYVNV	8	2	879.4932	-0.3	20.85	1	Q8VCP8	26		14.6
25.	SGLVYKNV	8	2	879.4922	-1.47	20.64	1	Q80TI1	26		30.4
26.	SGNIFVASL	9	2	907.4867	-1.83	27.44	1	O88495	25		35.8
27.	SIVSYNHL	8	2	932.4822	-1.5	22.3	1	Q9JHU9	21		10.2
28.	SNPEFRQL	8	2	990.4994	-0.99	18.61	1	Q3UWM4	27		17.3
29.	SSGDFPSL	8	1	809.3663	-1.58	32.32	1	Q9WVK4	24		138.2
30.	SSYNYRVV	8	2	987.4875	-1.98	18.4	1	P11881	26		5.4
31.	STFSFTKV	8	2	916.4765	-1.09	25.63	1	Q3TZZ7	21		7.7
32.	TTYKYEMI	8	2	1048.502	-0.21	24.58	1	Q8QZY1	28		28.6
33.	VFTEVANL	8	1	892.4758	-1.94	34.23	1	Q62141	22		195.2
34.	VFYEREVQM	9	2	1200.569	-2.64	25.49	1	Q80SY3	31		86.2
35.	VGINYREV	8	2	949.5077	-2.65	20.47	1	Q01320	22		46.2
36.	VNFEFPEF	8	2	1028.47	-1.98	50.37	1	P62082	22		43.3
37.	VNILENYL	8	2	977.5284	-1.93	31.24	1	Q64435	22		402.5
38.	VNIQYEVI	8	2	977.5284	-1.93	31.24	1	Q60961	25		324.5
39.	VNIQYLDL	8	2	977.529	-1.24	31.14	1	Q8R0G9	21		17
40.	AIYAFSHL	8	2	921.482	-1	30.93	1	Q9JJ59		0	2.2
41.	GTYDYTQL	8	1	960.4302	-0.77	30.12	1	Q8K2A8		0	31.7
42.	RAPVYARI	8	2	945.5602	-2.83	13.58	1	P52840		0	25
43.	RAYLFAHV	8	2	976.5349	-1.48	22.42	1	Q5SWD9		0	2.5
44.	RVYEFTRA	8	2	1041.546	-1.74	13.38	1	Q8VI38		0.049	45.2
45.	SGYDYYHV	8	2	1003.415	-0.8	22.78	1	O08785		0	6.9

46.	SQYRFEHL	8	2	1079.525	-1.46	17.98	1	Q3UJK4		0	3.8
47.	SSPKFSEI	8	2	894.4559	-1.01	18.91	1	Q91VM3		0	53.5
48.	AAYGFRNI	8	2	911.4717	-1.91	23.04	1	Q9CYQ7	30	0	9.6
49.	IGPRYSSV	8	2	878.4706	-2.85	15.19	1	Q5PRF0	26	0	19.4
50.	SAPLYTNL	8	1	878.46	-2.13	31	1	Q8K4S1	25	0	4.6
51.	SAYEVIKL	8	2	922.5235	-1.04	28.57	2	P06151,P16125	38	0	56.8
52.	STFVYNTM	8	1	962.4263	-2.65	29.89	1	Q8CFB4	38	0	7.7
53.	**SAYEFYHA**	**8**	**2**	**987.4195**	**-1.22**	**22.43**	**1**	**P97481**	**26**		**13**
54.	**SGTQYFRV**	**8**	**2**	**957.477**	**-1.99**	**19.42**	**1**	**P97412**	**21**		**201.2**
55.	**SLYQPAGL**	**8**	**1**	**848.4503**	**-1.12**	**31**	**1**	**P19096**	**40**		**70.7**
56.	**SSPHYTTL**	**8**	**2**	**905.4344**	**-2.16**	**14.13**	**1**	**P27046**		**0**	**12.2**
57.	**STTVFHSL**	**8**	**2**	**891.4551**	**-2.26**	**21.06**	**1**	**P19096**		**0**	**44.2**

Note: five of the peptides highlighted in red color did not display HFD VAT MIP specificity at the source protein level.

Table S4. Peptides and their potential source proteins found to be exclusively expressed in VAT MIP from HFD-induced obese mice as described in Section 2, Related to Figure 2

Peptide			Source Protein		
Sequence	Length	Affinity(nM)	Accession No	Name	Peptide Position
				Proteins involved in Glucose metabolism	
AAVKFHNL	8	15.8	Q64521	Glycerol-3-phosphate dehydrogenase 2	450-457
DFFNYAGL	8	43.4	P12265	Beta-glucuronidase	206-213
IGPYFEHNM	9	60.6	Q8VCB3	Glycogen synthase 2	66-74
SAYEVIKL	8	56.8	P06151	L-lactate dehydrogenase A chain	237-244
			P16125	L-lactate dehydrogenase B chain	238-245
				Proteins involved in lipid metabolic process	
ASTIAYLAL	9	252.5	O70503	17-beta-hydroxysteroid dehydrogenase 12	16-24
ISDVRVTQL	9	355.6	P55065	Phospholipid transfer protein	65-73
RAPVYARI	8	25	P52840	Sulfotransferase 1A1	68-75
RVYEFTRA	8	45.2	Q8VI38	Forssman glycolipid synthase	271-278
SAPLYTNL	8	4.6	Q8K4S1	Phosphoinositide phospholipase C-epsilon-1	1232-1239
SIVSYNHL	8	10.2	Q9JHU9	Inositol-3-phosphate synthase 1	328-335
STFSFTKV	8	7.7	Q3TZZ7	Extended synaptotagmin-2	157-164
				Proteins involved in protein metabolism	
AAYEFTTL	8	3.3	P32233	Developmentally-regulated GTP-binding protein 1	92-99
NSFRYNGL	8	9.3	P41105	60S ribosomal protein L28	36-43
SNPEFRQL	8	17.3	Q3UWM4	Lysine-specific demethylase 7A	775-782
SQYRFEHL	8	3.8	Q3UJK4	GTP-binding protein 2 (GTP-binding-like protein 2)	78-85
SSPKFSEI	8	53.5	Q91VM3	WD repeat domain phosphoinositide-interacting protein 4	70-77
TTYKYEMI	8	28.6	Q8QZY1	Eukaryotic translation initiation factor 3 subunit L	353-360

VFTEVANL	8	195.2	Q62141	Paired amphipathic helix protein Sin3b	205-212
VNFEFPEF	8	43.3	P62082	40S ribosomal protein S7	185-192
				Proteins involved in establishment of localization	
AIYAFSHL	8	2.2	Q9JJ59	ATP-binding cassette sub-family B member 9	23-30
IGPRYSSV	8	19.4	Q5PRF0	HEAT repeat-containing protein 5A	1980-1987
			Q6Q477	Plasma membrane calcium-transporting ATPase 4	565-572
KVYTFNSV	8	10.5	Q9R0K7	Plasma membrane calcium-transporting ATPase 2	553-560
			G5E829	Plasma membrane calcium-transporting ATPase 1	574-581
LAPVYQRL	8	17.7	P82198	Transforming growth factor-beta-induced protein ig-h3	670-677
QNYTYSSL	8	3.9	Q810S1	Calcium uniporter regulatory subunit MCUb	281-288
RSYDFEFM	8	21.5	P40336	Vacuolar protein sorting-associated protein 26A	105-112
VFYEREVQM	9	86.2	Q80SY3	V-type proton ATPase subunit d 2	292-300
VNIQYLDL	8	17	Q8R0G9	Nuclear pore complex protein Nup133	337-344
				Proteins involved in response to stimulus	
AALIYTSV	8	67.9	Q6PDL0	Cytoplasmic dynein 1 light intermediate chain 2	267-274
			Q8R1Q8	Cytoplasmic dynein 1 light intermediate chain 1	280-287
ANVQYMRV	8	31.8	Q61805	Lipopolysaccharide-binding protein	474-481
GQYEFHSL	8	91.9			74-81
ASVVFNQL	8	10.9	Q64288	Olfactory marker protein	156-163
ATLRYASL	8	3.9	Q9DBR4	Amyloid-beta A4 precursor protein-binding family B member 2	387-394
FAASYSAL	8	81.8	Q8BFW3	Protein phosphatase 1 regulatory subunit 15B	93-100
KSYLMNKL	8	29.4	Q8CFB4	Guanylate-binding protein 5	51-58
STFVYNTM	8	7.7			124-131
LAAQFSQL	8	62	Q9DCB4	cAMP-regulated phosphoprotein 21	547-554
SAPQFSKL	8	13.9	Q8K007	Extracellular sulfatase Sulf-1	230-237
SAPQYSRL	8	8.1	Q8CFG0	Extracellular sulfatase Sulf-2	231-238

SAYQRGESL	9	233.2	O35382	Exocyst complex component 4	322-330
SGNIFVASL	9	35.8	O88495	G protein-coupled receptor 50	70-78
SGYDYYHV	8	6.9	O08785	Circadian locomoter output cycles protein kaput	308-315
SSGDFPSL	8	138.2	Q9WVK4	EH domain-containing protein 1	349-356
SSYNYRVV	8	5.4	P11881	Inositol 1,4,5-trisphosphate receptor type 1	1169-1176
VGINYREV	8	46.2	Q01320	DNA topoisomerase 2-alpha	67-74
VNILENYL	8	402.5	Q64435	UDP-glucuronosyltransferase 1-6	214-221
				Others	
AAYGFRNI	8	9.6	Q9CYQ7	Nuclear prelamin A recognition factor	351-358
GTYDYTQL	8	31.7	Q8K2A8	Dol-P-Man:Man(5)GlcNAc(2)-PP-Dol alpha-1,3-mannosyltransferase	84-91
KSYDMSQV	8	199.4	Q8C8J0	Sperm-tail PG-rich repeat-containing protein 2	431-438
RAYLFAHV	8	2.5	Q5SWD9	Pre-rRNA-processing protein TSR1 homolog	250-257
SGLKYVNV	8	14.6	Q8VCP8	Adenylate kinase isoenzyme 6	27-34
SGLVYKNV	8	30.4	Q80TI1	Pleckstrin homology domain-containing family H member 1	460-467
VNIQYEVI	8	324.5	Q60961	Lysosomal-associated transmembrane protein 4A	60-67

Note: peptides sequence, length, predicted H2-Kb-binding affinity (IC_{50}), protein name, accession number and function, according to Uniprot database are listed.

Table S5. Several known obesity-associated proteins are detected in the obese VAT-exclusive MIPs source proteome, Related to Figure 2

Protein ID	Protein name (gene)	Functions	Obesity-association	References
Q61805	Lipopolysaccharide-binding protein (Lbp)	Lipid binding	LBP is an inflammatory marker associated with obesity-related insulin resistance	(Kim et al., 2016; Moreno-Navarrete et al., 2012)
O88495	Melatonin-related receptor (Gpr50)	G-protein coupled receptor activity; regulating energy metabolism	GPR50 knockout mice were partially resistant to diet-induced obesity.	(Ivanova et al., 2008).
P55065	Phospholipid transfer protein (Pltp)	lipid transporter activity	PLTP mass and activity have been found to be elevated in the plasma of type 2 diabetes mellitus (T2DM) and obese patients. PLTP mass and activity have been found to be positively associated with BMI, fat mass and leptin levels. PLTP activity is independently associated with nonalcoholic fatty liver disease.	(Qin et al., 2014) (Tzotzas et al., 2009)
Q8VCB3	Glycogen synthase 2 (Gys2)	Glucose binding	GYS2 as a novel genetic factor for polycystic ovary syndrome through obesity-related condition.	(Hwang et al., 2012)

Q8CFG0	Extracellular sulfatase Sulf-2 (Sulf2)	arylsulfatase activity	SULF2 strongly predisposes to fasting and postprandial triglycerides in patients with obesity and type 2 diabetes mellitus.	(Hassing et al., 2014)
P06151	L-lactate dehydrogenase A chain (Ldha)	pyruvate fermentation to lactate	Lactate dehydrogenase gene is downregulated in visceral white adipose tissue of HFD-fed rats, suggesting a decreased anaerobic degradation of glucose in adipose tissue. As a result, pyruvate would be directed to acetyl-CoA production, which in turn would fuel fatty acid biosynthesis and triglyceride storage. However, it has also been reported that activating or overexpressing LDH-A react against lipid accumulation by deviating pyruvate to lactate. Lactate increases the destiny of white adipose cells towards a brown phenotype. The elevated level of LDHA has been suggested to be related with the reduction of body weight gain.	(Lopez et al., 2004; Parray and Yun, 2015)
Q64521	Glycerol-3-phosphate dehydrogenase 2, mitochondrial (Gpd2)	Calcium ion binding; gluconeogenesis; NADH metabolic process	Mitochondrial glycerol 3-phosphate dehydrogenase (mGPDH) is an integral component of the respiratory chain. Lou/C, a rat strain derived from Wistar, is resistant to age- and diet-related obesity, and this feature has been shown to be linked to a high expression and activity of mitochondrial glycerol-3-phosphate dehydrogenase. Deficiency of the mitochondrial glycerol 3-phosphate dehydrogenase contributes to hepatic steatosis.	(Taleux et al., 2009) (Zheng et al., 2019)

Table S6. Selected potential candidate peptides for immunogenicity evaluation, Related to Figure 3 and Figure 4

Group	Name	Source protein	Protein_ID	Function	Sequence	IC50(nM)	HFD-VAT MIP	NCD-VAT MIP
G1	DHB_{16-24}	17-beta-hydroxys-teroid dehydrogenase 12	O70503	Oxidoreductase; lipid metabolism	ATLRYASL	252.2	+	-
	LBP_{74-81}	Lipopolysaccharide-binding protein	Q61805	Lipid binding; immune system process; response to stimulus	GQYEFHSL	91.9	+	-
	$LDHA_{237-244}$	L-lactate dehydrogenase A or B chain	P06151	Oxidoreductase; glucose metabolism; response to stimulus	SAYEVIKL	56.8	+	-
	$APBB2_{387-394}$	Amyloid-beta A4 precursor protein-binding family B member 2	Q9DBR4	Nucleic acid-templated transcription; response to stimulus	ATLRYASL	3.9	+	-
	$V\text{-}ATPase_{292-300}$	V-type proton ATPase subunit d 2	Q80SY3	Hydrolase	VFYEREVQM	86.2	+	-

G2	ITPR1$_{1169-1176}$	Inositol 1,4,5-trisphosphate receptor type 1	P11881	Calcium ion transport	SSYNYRVV	5.4	+	-
	EXOC4$_{322-330}$	Exocyst complex component 4	O35382	Golgi to plasma membrane transport	SAYQRGESL	233.2	+	-
	GBP5$_{124-131}$	Guanylate-binding protein 5	Q8CFB4	GTPase activity	STFVYNTM	7.7	+	-
	AK6$_{10-17}$	Adenylate kinase isoenzyme 6	Q8VCP8	ATPase activity	SGLKYVNV	14.6	+	-
	EHD1$_{349-356}$	EH domain-containing protein 1	Q9WVK4	ATP/GTP binding; calcium ion binding	SSGDFPSL	138.2	+	-
G3	CATA$_{384-392}$	Catalase	P24270	Cholesterol metabolic process	ANYQRDGPM	214.7	+++	+
	PLIN2$_{213-221}$	Perilipin-2	P43883	Lipid storage; long-chain fatty acid transport	SNYERLESL	64.4	+++	+
	D19L3$_{433-440}$	Probable C-mannosyltransferase DPY19L3	Q71B07	Transferase activity	SVVAFHNL	8.69	+++++++	+

Note: a plus or multiple plus indicates the abundance of the indicated peptide in the given tissue-derived MIP; the minus sign indicates that the indicated peptide cannot be detected in the given tissue-derived MIP.

Transparent Methods

Animal models

Four-week-old male C57BL/6J wild-type mice (HFK Bioscience, Beijing, China) were maintained under a 12 h light-dark cycle in specific pathogen-free facilities, and were allowed free access to sterilized water and to either a high fat diet (HFD, D12492, 60 Kcal% fat, Research Diets) or a normal chow diet (NCD, D12450B 10 Kcal% fat, Research Diets). For the glucose tolerance test (GTT), the mice were made to fast for 16 h prior to intraperitoneal administration of glucose (1g kg^{-1}). Blood glucose was measured from tail vein at indicated time points with a glucometer (ONETOUCH Ultra). For the insulin tolerance test (ITT), mice were made to fast for 4 h prior to intraperitoneal administration of insulin (Novolin; 0.75U kg^{-1}) and blood glucose concentrations were measured at indicated time points. All procedures were approved by the Institute Animal Care and Use Committee of the Third Military Medical University (Chongqing, China).

Isolation of MIP from VAT

The epididymal fat pad (VAT samples) (total 28 g) were collected from 25 HFD-fed obese male mice or 75 NCD-fed lean male mice at 12 weeks of age from three different batches, respectively, and immediately lysed in 40 ml of ice-cold lysis buffer (50 mM Tris-HCl, 150 mM NaCl, and 1% of CHAPS, pH 8.0) containing “complete” protease inhibitor (Roche). Cell lysates were clarified by several rounds of centrifugation (12000g, 30 min, 4°C), and the supernatant was collected and used for immunoaffinity chromatography. The MIPs were isolated following a method described previously (Delgado et al., 2009; Escobar et al., 2008; Purcell, 2004) with some modifications. Initially, immunoaffinity columns were constructed

based on the following steps: 1) the top-cap of 1 ml HiTrap NHS-activated HP column (Code No:17-0716-01, GE Healthcare) was removed and a drop of ice-cold 1 mM HCl was introduced into the top to avoid air bubble formation; 2) 3 × 2 ml ice-cold 1 mM HCl was injected to wash out the isopropanol in the column at a flow rate not exceeding 1 ml/min. 3) For antibody coupling, 10 ml of 1 mg/ml anti-H2-Kb mAb (clone: Y-3, Bioxcell company) antibody in coupling buffer (0.2 M NaHCO3, 0.5 M NaCl, pH 8.3) was passed through the column repeatedly at a flow rate of 1 ml/min for 4 h at 4 °C. 4) To deactivate any excess active groups that had not coupled to the ligand and to wash out the non-specifically bound ligands, 3 × 2 ml of Buffer A (0.5 M ethanolamine, 0.5 M NaCl, pH 8.3) and 3 × 2 ml of Buffer B (0.1 M sodium acetate, 0.5 M NaCl, pH 4) were injected into the column alternately; after the columns were maintained at room temperature for 15–30 min, 3 × 2 ml of Buffer B and 3 × 2 ml of Buffer A were injected into the column alternately; 15 ml of lysis buffer (50 mM Tris-HCl, pH 8.0 150 mM NaCl and 1% of CHAPS) was injected into the column. Next, the VAT proteolytic solution was repeatedly circulated in the column overnight at a flow rate of 1 ml/min at 4°C. Following this, the column was washed with several buffers in the following order: 15 ml of wash buffer 1 (50 mM Tris-HCl, pH 8.0, 150 mM NaCl, and 1% of CHAPS), 15 ml of wash buffer 2 (50 mM Tris-HCl, pH 8.0, 150 mM NaCl in deionized H_2O), 25 ml of wash buffer 3 (50 mM Tris-HCl, pH 8.0, 450 mM NaCl in deionized H_2O), and 35 ml of wash buffer 4 (50 mM Tris-HCl, pH 8.0, in deionized H_2O). Subsequently, the HLA-peptide complexes were eluted with 6 ml of 10% acetic acid. The ultrafiltration filters (3.0-kDa cutoff Microcon, Millipore) were prewashed with 0.1 N acetic acid and 10% acetonitrile to remove contaminants interfering with the mass spectrometry, and the mixture of peptides and class I heavy-chain and β2-microglobulin were

separated by ultrafiltration at 10000 × g (Escobar et al., 2008; Murphy et al., 2017). After ultrafiltration, the peptides mixtures were desalinated and concentrated by Micro-Tip reversed-phase C18 columns (Merck) (Bassani-Sternberg et al., 2010). The C18 columns were washed with 80% acetonitrile in 0.1% TFA, equilibrated with 0.1% TFA, and loaded with the peptide mixture. The C18 columns were washed additionally by 0.1% TFA. Lastly, the peptides were eluted with 400 μl 80% acetonitrile in 0.1% TFA, and all peptide elutions were vacuum concentrated to a final volume of 20 μl prior to mass spectrometry analysis.

MIP analysis using LC-MS/MS

MIP samples were loaded into an analytical column (Acclaim™ PepMap™ 100, 75 μm ×15 cm, C18, 3 μm, 100 Å, Thermo Fisher Scientific) with a Trap Column (Acclaim™ PepMap™ 100, 75 μm×2 cm, C18, 3 μm, 100 Å, Thermo Fisher Scientific) and separated by reversed-phase chromatography (Easy nanoLC1000, Thermo Fisher Scientific) using a 120 min gradient at a flow rate of 300 nL/min. The gradient was composed of Solvent A (0.1% formic acid in water) and Solvent B (0.1% formic acid in acetonitrile); the elution gradient was as follows: 2-7% B in 3 min, 7-22% B in 96 min, 22-35% B in 10 min, 35-90% B in 2 min, 90% B for 5 min and 90-2% B in 2 min, 2% B for 2 min. The eluted peptides were sprayed into the LTQ Orbitrap using nano-electron spray ionization (NSI) at a capillary voltage of 2.5 KV and 300 ℃capillary temperature. The instrument was operated in the data-dependent mode. Survey MS spectra from 350.0–1800.0 m/z were obtained in the orbitrap at 60,000 M/ΔM resolution, followed by data dependent acquisition (DDA) of the top 16 most abundant precursor ions with an isolation window of 2.0 m/z, and followed by MS/MS scans of the ion trap using product ion scans (relative CID energy 35) of the top 16 most abundant precursor ions in the survey scan. MS

scans were captured in profile mode, while the MS/MS scans was captured in centroid mode. The product ion scans were obtained using a 2.0-unit isolation width and normalized collision energy of 35 in an LTQ Orbitrap Velos Pro MS spectrometer (Thermo Fisher Scientific). Three replicate injections were performed for each set of samples.

Database search and spectral annotation

Acquired tandem mass spectrometric spectra were searched using Mascot (version 2.3, Matrix Science) and the Sequest HT search engine with the Proteome Discoverer software (PD) (version 1.4.0.288, Thermo Fisher Scientific) against the UniProt mouse FASTA protein database and reversed decoy sequences. MS/MS spectra were captured in CID mode. Mascot search parameters were set as follows: precursor ion mass tolerance 5 ppm, fragment ion mass tolerance 0.8Da, no enzyme specificity, oxidized methionine was allowed as a dynamic modification, FDR<5% (peptide-spectrum match level). Protein grouping was disabled, allowing multiple annotations of peptides (for example, conserved sequence mapping into multiple proteins). The Sequest HT used the same search parameters as Mascot. Mascot and Sequenst search results in technical triplicates were combined to establish datasets of HFD VAT MIP and NCD VAT MIP. Firstly, peptides with either an Ionscore>20 in Mascot search (Al-Shahib et al., 2010; Kowalewski and Stevanovic, 2013; Kumar et al., 2015; Ni et al., 2019) or a q-value<0.05 in Sequest search (Franchin et al., 2014; Kall et al., 2008) were collected. Secondly, peptide lengths were limited to 8-12 amino acids. Finally, high confidence H2-Kb-associated peptides were identified by IC_{50}<500 nM (NetMHC 4.0: http://www.cbs.dtu.dk/services/NetMHC/), (Andreatta and Nielsen, 2016)

Determination of MHC class I motifs

We used the weblogo program (http://weblogo.berkeley.edu/logo.cgi) to visualize the characteristics of the binding motifs. The information content at each position in the sequence motif corresponds to the height of a column of letters. The height of each letter within the column is proportional to the frequency of the corresponding amino acid at that position.

Annotation enrichment analysis and functional annotation of MIP source proteins

Biological annotation and KEGG pathway enrichment of the VAT MIP source proteins was performed using the R package “clusterProfiler” (version 3.10.1).Terms with adjusted P value < 0.01 were considered significant.

Peptide Synthesis

The peptides were synthesized at a purity>95% at the Chinese Peptide Company (Hangzhou, China). Synthetic peptides were used for validation of LC-MS/MS identification as well as for functional experiments.

H2-Kb binding assays

Peptide binding to H2-Kb was measured using the transporter associated with TAP-deficient RMAS cell line. Briefly, RMAS cells were cultured overnight in complete medium at 26 °C, 5% CO_2. The RMAS cells ($1x10^6$ cells/ml) were incubated with or without each peptide pool (total 100 μg/ml) for 3 h at 26 °C, followed by a second incubation for 3 h at 37 °C, 5% CO_2. An H2-Kb-binding LCMV peptide GP_{33-41} (KAVYNFATM) was used as a positive control. After incubation, the cells were washed twice with ice-cold PBS and stained with PE-conjugated anti-mouse H2-Kb mAb (eBioscience, AF6) for 30 min at 4 °C. The cells were washed and detected by flow cytometry (BD FACS Calibur). Data analysis was performed using the FlowJo software (v7.6.3, Treestar, San Carlos, CA, USA).

Amplification of Peptide-Specific $CD8^+$T Cells and intracellular cytokine staining

Splenocytes isolated from C57BL/6J mice were stimulated with each peptide pool or single peptide (100 μg/ml) in complete medium containing recombinant IL-2 (30 IU/ml; Roche), and half the medium was replaced with complete medium supplemented with IL-2 every 3–4 days. Cell cultures were restimulated with the peptide pool or single peptide (50 μg/ml)-pulsed RMAS cells or only RMAS cells on day 7. To block the H2-Kb-restricted recognition of $CD8^+$ T cells, anti-H2-Kb antibody Y-3 (10 μg/ml) was added to the cell cultures. The presence of peptide-specific $CD8^+$ T cells was assessed by intracellular IFN-γ and TNF-α staining. Two hours after the restimulation, 0.65μl ml^{-1}GolgiStop™ (BD Biosciences) was added into each culture at 37 °C and incubated for an additional 4 hours. Before staining, all cell preparations were incubated with anti-mouse CD16/32 (BD Biosciences) for 10 min on ice to block the Fc receptors. Dead cells were excluded from the analysis by using the fixable Viability Dye eFluor® 780 (eBioscience). Percp-cy5.5-conjugated CD3 mAb (clone:53-6.7 eBioscience) and FITC-conjugated anti-CD8α mAb (clone:17A2 eBioscience) were used to label cells for 30 min on ice. After washing with the flow cytometer buffer (PBS/1% FBS), cells were fixed and then labeled with PE-conjugated anti-mouse TNF-α (clone: MP6-XT22 eBioscience) or APC-conjugated anti-mouse IFN-γ (clone: XMG1.2 eBioscience) at 4 °C in a permeabilization buffer. PE or APC-conjugated isotype IgG1 was used as a negative staining control (eBioscience). Flow cytometry data were acquired for each of the experiments using a BD FACS Calibur (BD Biosciences, Franklin Lakes, NJ). Data analysis was performed using the FlowJo software.

Pentamer staining

Lymphocytes were isolated from the mesenteric lymph nodes of HFD-fed obese mice and NCD-fed lean mice post the 8-week feeding. A single cell suspension was prepared in PBS at a cell concentration of 1-2·10^6 cells/100 μl, initially stained with Fixable Viability Dye eFluor® 780 (eBioscience) and washed, and then stained with PE-conjugated pentamers (Proimmune,5 μl/test) for 15 min-incubation at 37 ºC in dark. After washing twice with FACS buffer, cells were incubated with FITC-conjugated-anti-mouse CD8 (clone: 17A2, eBioscience) at 4 ºC for 30 min. Cells were washed twice with FACS buffer, and fixed with 1% polyformaldehyde. After washing, stained cells were resuspended in 200-300 μl FACS buffer and measured using a BD FACS Calibur (BD Biosciences, Franklin Lakes, NJ).

Preparation of VAT-isolated stromal-vascular fractions (SVF)

Acquired epididymal VAT from HFD-fed obese mice and NCD-fed lean mice were divided into fine pieces in a weight boat containing 3 ml DPBS supplemented with 0.5% BSA. The VAT samples were then poured into 50 ml conical tubes, rinsed with 3 ml collagenase II digest solution consisting of 1X DPBS supplemented with 0.5% BSA, 10 mM CaCl2, and 4 mg/ml type II collagenase, and incubated in a rotational shaker (200 rpm, 37 ºC, 20 min). The VAT homogenate, along with 10 ml DPBS (0.5% BSA), was passed through a 100 μm filter into fresh 50 ml conical tubes. The VAT-isolated SVFs were obtained after centrifuging cell suspensions (500g, 4 ºC, 10 min) and discarding the supernatant. The VAT-isolated SVFs were restimulated with peptide (10 μg/ml)-pulsed RMAS cells or RMAS cells alone. The presence of peptide-specific $CD8^+$ T cells was assessed by intracellular IFN-γ and TNF-α staining.

Treatment of mice

C57BL/6J male mice administered HFD starting at 4 weeks of age were randomly divided into 4 groups (4-5 mice per group), two of which were administered 20 μg $LDHA_{237-244}$ peptide or PBS (once a day at day 1-5, 8, then once a week until the age of 12 weeks) intranasally, starting at 4 weeks of age, and the other two groups were injected intraperitoneally with 50 μg $LDHA_{237-244}$ peptide (twice a week for the first two weeks and once a week until the age of 12 weeks) or PBS simultaneously. Weight changes were monitored weekly until 12 weeks of age. GTT and ITT were measured at 12 weeks of age.

RNA Isolation and Quantitative Real-Time PCR

For real-time PCR, total RNA was extracted from 0.2 mg VAT using HiPure Universal RNA Kit(Magen company, Guangzhou, China). Real-time quantitative PCR was performed using TB Green™ Premix Ex Taq™ II (Tli RNaseH Plus) (Takara, Kyoto, Japan) for H2-Kb and TaqMan™ Gene Expression Master Mix (Applied Biosystems™, Foster City, CA, USA) for the other genes according to the manufacturer's instructions. The following primers were used: *H2-kb* (Fwd: ggctggtgaagcagagagac, Rev: cagcacctcagggtgacttt), *Ldha* (Mm01612132_g1, Thermo fisher), *Psmb1* (Mm00650840_m1, Thermo fisher), *Psmb2* (Mm00449477_m1, Thermo fisher), *Psmb8* (Mm00479004, Thermo fisher), *Psmb9* (Mm00440207, Thermo fisher), and *Psmb10* (Mm00479052_g1, Thermo fisher). Each sample run was performed in triplicate, and the relative mRNA expression levels were determined using the 2(-Delta Ct) method with *Gapdh* as the internal reference control.

Western bolt analysis

VAT from obese and lean mice were lysed in RIPA buffer (50 mM Tris-HCl pH 7.4, 1% Nonidet P-40,0.25% Na-deoxycholate, 150 mM NaCl, 1 mM EDTA) containing complete protease

inhibitor mixture (Roche Life Sciences), 1 mM Na3VO4 pH 9, 5 mM NaF, and 10 mM NEM (Sigma-Aldrich). H2-Kb molecules were separated from elution fractions using ultrafiltration with a 3-KDa cutoff. Samples were separated by SDS-PAGE and immunoblotted with the following primary antibodies: Rabbit polyclonal to MHC Class I H2-Kb (ab93364, Abcam), Rabbit monoclonal to mouse LDHA (ab101562, Abcam), and anti-mouse GAPDH antibody (ab181602, Abcam). After incubation with peroxidase-coupled secondary antibodies for 60 min, the immunocomplexes were visualized using a chemiluminescence reagent (Amersham, Freiburg, Germany), and the autoradiographs were scanned by an imaging densitometer.

Measurement of lactate dehydrogenase (LDH) activity

Total LDH activity in VAT was determined using the LDH activity assay kit (MAK06, Sigma) according to the manufacturer's protocol. Briefly, fresh VAT samples (100 mg) from HFD or NCD-fed mice were homogenized rapidly on ice in 500 μl of cold LDH Assay buffer and centrifuged at 10,000 g for 15 min at 4 °C to remove any insoluble materials; the soluble fraction was used for the assay. Changes in absorbance were determined by total LDH activity at 450 nm using BIO-RAD IMark™ Microplate Reader.

Immunoprecipitation and western blot analysis of ubiquitination

Pooled VAT tissues (0.5mg) from three or four obese or lean mice were washed twice with ice-cold PBS and lysed in 2 ml Triton-lysis buffer (20 mM Tris-HCl, pH 7.5, 150 mM NaCl, 5 mM EDTA, 2 mM dithiothreitol, 1%Triton X-100, 1% protease inhibitor cocktail, 1 mM PMSF) in the presence or absence of 10 μM MG132 (a proteasome inhibitor). The lysates were centrifuged at 12,000 × g for 10 min at 4 °C and the supernatant was precleared with 20 μL Protein A/G PLUS-Magnetic Beads (Thermo fisher) for 1 h at 4 °C. The lysates were

immunoprecipitated overnight with LDHA-specific rabbit polyclonal antibody (19987-1-AP, proteintech, 2 μg/test) at 4 °C, followed by incubation with protein A/G Magnetic Beads. This was followed by four washes with ice-cold lysis buffer and elution in 2X SDS sample buffer. The immunoprecipitates were boiled in 2X SDS sample buffer, resolved by SDS-PAGE, and subjected to overnight immunoblotting with specific antibodies against Lys48-specific Ubiquitin (clone: Apu2, Millipore, 1:1000) or LDHA (clone: EPR1563Y, Abcam, 1:1000) at 4 °C. Proteins were visualized using a goat anti-rabbit secondary antibody conjugated to HRP (D110058-0100, shanghai shengong company, 1:5000, 1 hour at room temperature) and a chemiluminescence detection system.

Statistical analysis

We used the Prism5 software (GraphPad Software) for all statistical tests. The unpaired two-group comparison was conducted using Student's t-test. Data were presented as the mean ± SD. $P<0.05$ (*), $P<0.01$ (**) and $P<0.001$(***) were considered statistically significant.

References:

Al-Shahib, A., Misra, R., Ahmod, N., Fang, M., Shah, H., and Gharbia, S. (2010). Coherent pipeline for biomarker discovery using mass spectrometry and bioinformatics. BMC Bioinformatics *11*, 437.

Andreatta, M., and Nielsen, M. (2016). Gapped sequence alignment using artificial neural networks: application to the MHC class I system. Bioinformatics *32*, 511-517.

Bassani-Sternberg, M., Barnea, E., Beer, I., Avivi, I., Katz, T., and Admon, A. (2010). Soluble plasma HLA peptidome as a potential source for cancer biomarkers. Proc Natl Acad Sci U S A *107*, 18769-18776.

Delgado, J.C., Escobar, H., Crockett, D.K., Reyes-Vargas, E., and Jensen, P.E. (2009). Identification of naturally processed ligands in the C57BL/6 mouse using large-scale mass spectrometric peptide sequencing and bioinformatics prediction. Immunogenetics *61*, 241-246.

Escobar, H., Crockett, D.K., Reyes-Vargas, E., Baena, A., Rockwood, A.L., Jensen, P.E., and Delgado, J.C. (2008). Large scale mass spectrometric profiling of peptides eluted from HLA molecules reveals N-terminal-extended peptide motifs. J Immunol *181*, 4874-4882.

Franchin, C., Pivato, M., Rattazzi, M., Arrigoni, G., and Millioni, R. (2014). OFFGEL fractionation of peptides: where really is your sample? J Chromatogr A *1355*, 278-283.

Hassing, H.C., Surendran, R.P., Derudas, B., Verrijken, A., Francque, S.M., Mooij, H.L., Bernelot Moens, S.J., Hart, L.M., Nijpels, G., Dekker, J.M., et al. (2014). SULF2 strongly prediposes to fasting and postprandial triglycerides in patients with obesity and type 2 diabetes mellitus. Obesity *22*, 1309-1316.

Hwang, J.Y., Lee, E.J., Jin Go, M., Sung, Y.A., Lee, H.J., Heon Kwak, S., Jang, H.C., Soo Park, K., Lee, H.J., Byul Jang, H., et al. (2012). Genome-wide association study identifies GYS2 as a novel genetic factor for polycystic ovary syndrome through obesity-related condition. Journal of human genetics *57*, 660-664.

Ivanova, E.A., Bechtold, D.A., Dupre, S.M., Brennand, J., Barrett, P., Luckman, S.M., and Loudon, A.S. (2008). Altered metabolism in the melatonin-related receptor (GPR50) knockout mouse. American journal of physiology. Endocrinology and metabolism *294*, E176-182.

Kall, L., Storey, J.D., MacCoss, M.J., and Noble, W.S. (2008). Posterior error probabilities and false discovery rates: two sides of the same coin. J Proteome Res *7*, 40-44.

Kim, K.E., Cho, Y.S., Baek, K.S., Li, L., Baek, K.H., Kim, J.H., Kim, H.S., and Sheen, Y.H. (2016). Lipopolysaccharide-binding protein plasma levels as a biomarker of obesity-related insulin resistance in adolescents. Korean journal of pediatrics *59*, 231-238.

Kowalewski, D.J., and Stevanovic, S. (2013). Biochemical large-scale identification of MHC class I ligands. Methods Mol Biol *960*, 145-157.

Kumar, G., Gotesman, M., and El-Matbouli, M. (2015). Interaction of Tetracapsuloides bryosalmonae, the causative agent of proliferative kidney disease, with host proteins in the kidney of Salmo trutta. Parasitol Res *114*, 1721-1727.

Lopez, I.P., Milagro, F.I., Marti, A., Moreno-Aliaga, M.J., Martinez, J.A., and De Miguel, C. (2004). Gene expression changes in rat white adipose tissue after a high-fat diet determined by differential display. Biochemical and biophysical research communications *318*, 234-239.

Moreno-Navarrete, J.M., Ortega, F., Serino, M., Luche, E., Waget, A., Pardo, G., Salvador, J., Ricart, W., Fruhbeck, G., Burcelin, R., et al. (2012). Circulating lipopolysaccharide-binding protein (LBP) as a marker of obesity-related insulin resistance. International journal of obesity *36*, 1442-1449.

Murphy, J.P., Konda, P., Kowalewski, D.J., Schuster, H., Clements, D., Kim, Y., Cohen, A.M., Sharif, T., Nielsen, M., Stevanovic, S., et al. (2017). MHC-I Ligand Discovery Using Targeted Database Searches of Mass Spectrometry Data: Implications for T-Cell Immunotherapies. J Proteome Res *16*, 1806-1816.

Ni, X., Tan, Z., Ding, C., Zhang, C., Song, L., Yang, S., Liu, M., Jia, R., Zhao, C., Song, L., et al. (2019). A region-resolved mucosa proteome of the human stomach. Nat Commun *10*, 39.

Parray, H.A., and Yun, J.W. (2015). Proteomic Identification of Target Proteins of Thiodigalactoside in White Adipose Tissue from Diet-Induced Obese Rats. International journal of molecular sciences *16*, 14441-14463.

Purcell, A.W. (2004). Isolation and characterization of naturally processed MHC-bound peptides from the surface of antigen-presenting cells. Methods Mol Biol *251*, 291-306.

Qin, S., Song, G., and Yu, Y. (2014). Phospholipid transfer protein in diabetes, metabolic syndrome and obesity. Cardiovascular & hematological disorders drug targets *14*, 149-153.

Taleux, N., Guigas, B., Dubouchaud, H., Moreno, M., Weitzel, J.M., Goglia, F., Favier, R., and Leverve, X.M. (2009). High expression of thyroid hormone receptors and mitochondrial glycerol-3-phosphate dehydrogenase in the liver is linked to enhanced fatty acid oxidation in Lou/C, a rat strain resistant to obesity. The Journal of biological chemistry *284*, 4308-4316.

Tzotzas, T., Desrumaux, C., and Lagrost, L. (2009). Plasma phospholipid transfer protein (PLTP): review of an emerging cardiometabolic risk factor. Obesity reviews : an official journal of the International Association for the Study of Obesity *10*, 403-411.

Zheng, Y., Qu, H., Xiong, X., Wang, Y., Liu, X., Zhang, L., Liao, X., Liao, Q., Sun, Z., Ouyang, Q., et al. (2019). Deficiency of Mitochondrial Glycerol 3-Phosphate Dehydrogenase Contributes to Hepatic Steatosis. Hepatology *70*, 84-97.

iScience, Volume *23*

Supplemental Information

Obesity Reshapes Visceral Fat-Derived MHC I Associated-Immunopeptidomes and Generates Antigenic Peptides to Drive $CD8^+$ T Cell Responses

Xiaoling Chen, Shufeng Wang, Yi Huang, Xia Zhao, Xu Jia, Gang Meng, Qian Zheng, Mengjun Zhang, Yuzhang Wu, and Li Wang

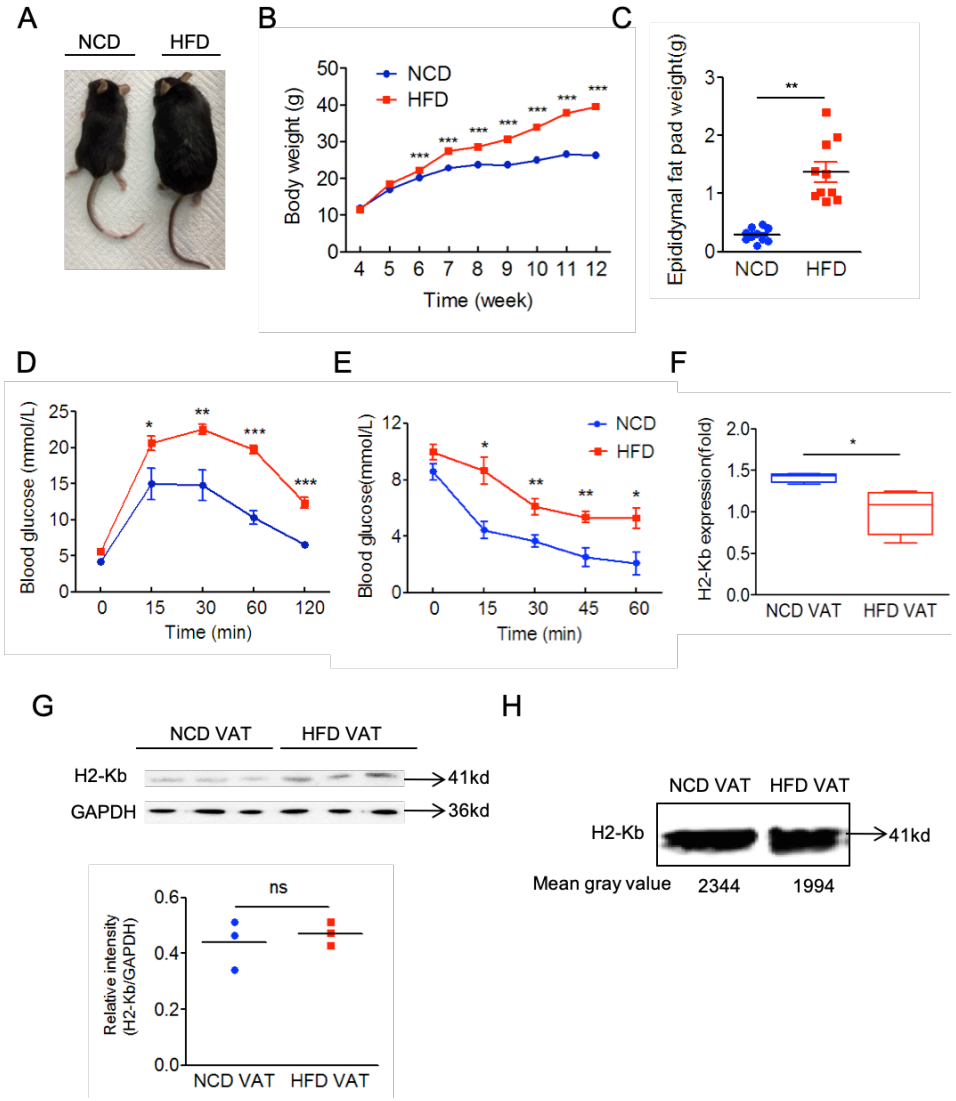

Figure S1. Establishment of high fat diet (HFD)-induced obese C57BL/6 mice model, Related to Figure 1

(A) Representative images of C57BL/6 male mice fed with a high-fat diet (HFD) or a normal diet (NCD) beginning at 4 weeks of age for 8 weeks. (B) Body weight gain of male C57BL/6 mice after 8-week HFD or NCD feeding (started at 4 weeks of age) (n=10 mice per group). The epididymal fat pad (VAT) mass from male C57BL/6 mice with HFD or NCD feeding at 12 weeks of age. (n=10 mice per group). Serum glucose levels during (D) glucose tolerance test (GTT) and (E) insulin tolerance test (ITT) in male C57BL/6 mice after 8-week HFD (n=10 mice per group). Data are means and error bars are ±SEM. Quantitative real-time PCR analysis (n=10 mice per group) (F) and immunoblotting analyses (n=3 mice per group) (G) of H2-Kb expression in the VAT of mice after 8-week HFD or NCD feeding. (H) Immunoblotting analyses of H2-Kb in Co-IP ultrafiltration superfluid from the VAT homogenates of mice after 8-week HFD or NCD feeding.

* $p < 0.05$, ** $p < 0.01$, *** $p<0.0001$, and ns: no significance, determined by Student's t-test.

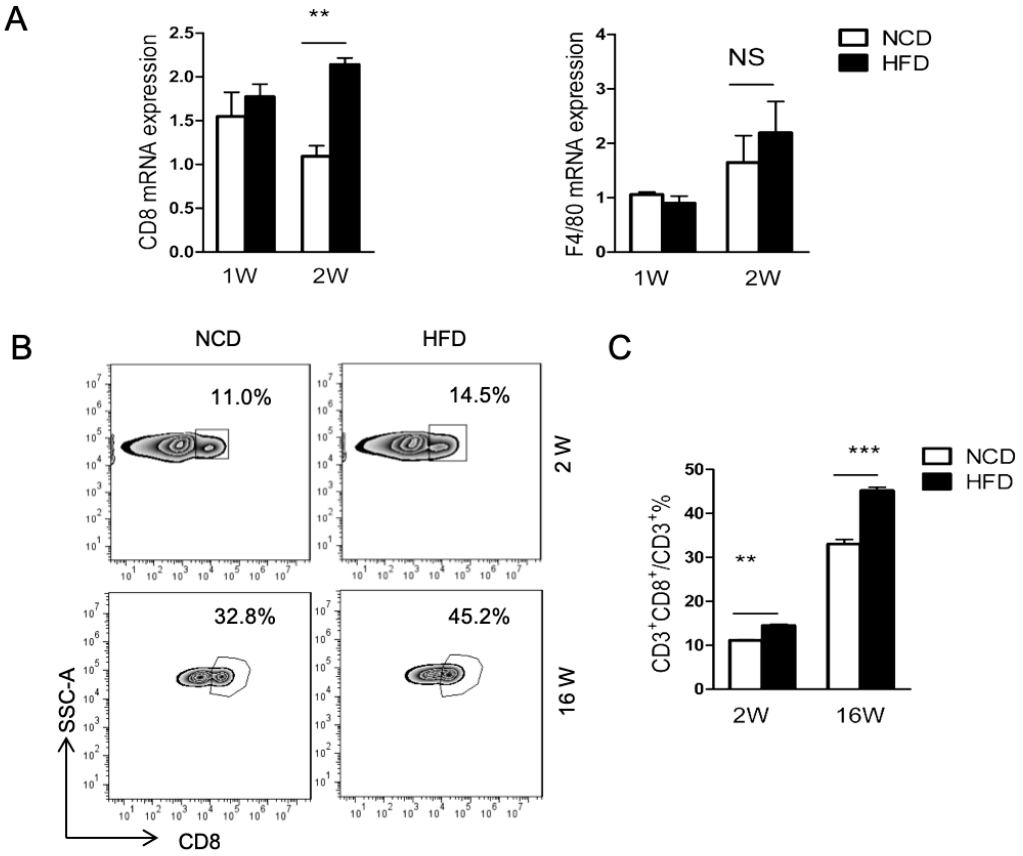

Figure S2. HFD feeding induces an early increase of $CD8^+$ T cells in visceral adipose tissues, Related to Figure 3

(A) Quantitative real-time PCR analysis of CD8 and F4/80 expression in the epididymal fat pads from mice fed with NCD and HFD for 1 or 2 weeks (started at 4 weeks of age) (n=10 mice per group). Data are means and error bars are ±SEM. Student's t test, *p < 0.05 and **p < 0.01, ***P<0.0001

(B) Representative FACS analysis of the proportion of infiltrated CD8+ T cells in the epididymal fat pads from mice fed with NCD and HFD for 2 or 16 weeks (started at 4 weeks of age). (C) Summary graph for FACS analysis of the frequency of infiltrated CD8+ T cells in the epididymal fat pads from mice fed with NCD and HFD for 2 and 16 weeks. Data are means and error bars are ±SEM.

* p < 0.05, ** p < 0.01, *** p<0.0001, and NS: no significance, determined by Student's t-test.

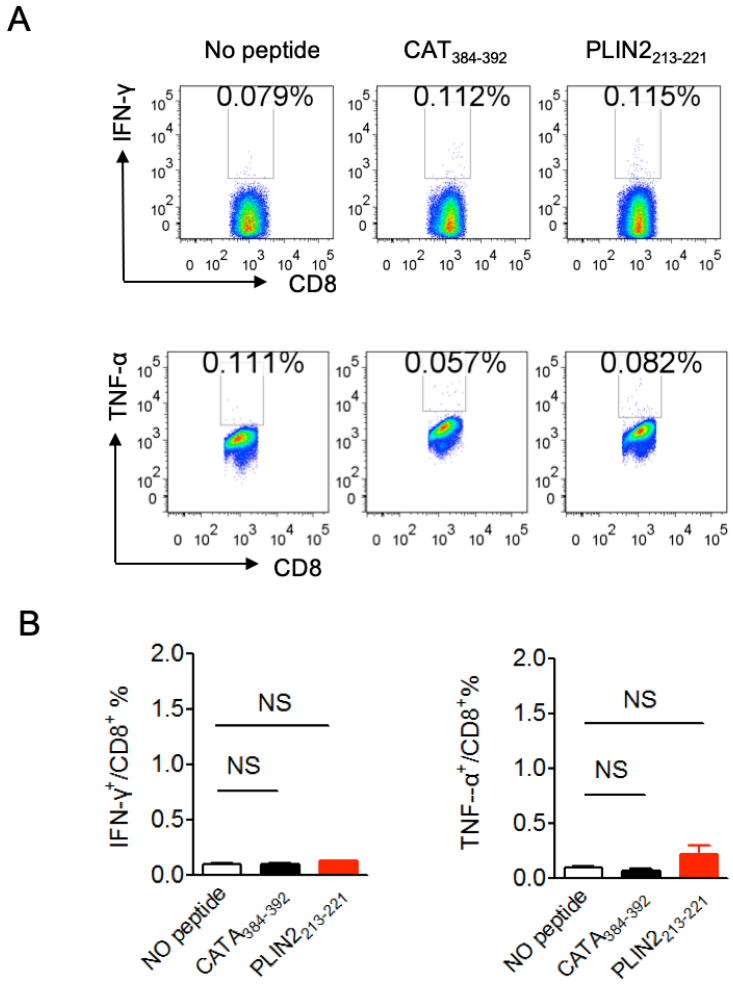

Figure S3. The peptides shared by VAT-MIPs from both NCD and HFD-fed mice have no ability to prime CD8$^+$ T cells response, Related to Figure 4

(A) Representative FACS plots indicating intracellular IFN-γ and TNF-α staining of CD8$^+$ T cells stimulated with the indicated peptides-loaded RAMS cells.

(B) Summary graph for FACS analysis of the frequency of IFN-γ and TNF-α-producing cells among CD8$^+$ T cells stimulated with the indicated peptides. Each bar represents the mean ± SEM of three independent experiments. NS: no significance, determined by Student's t-test.

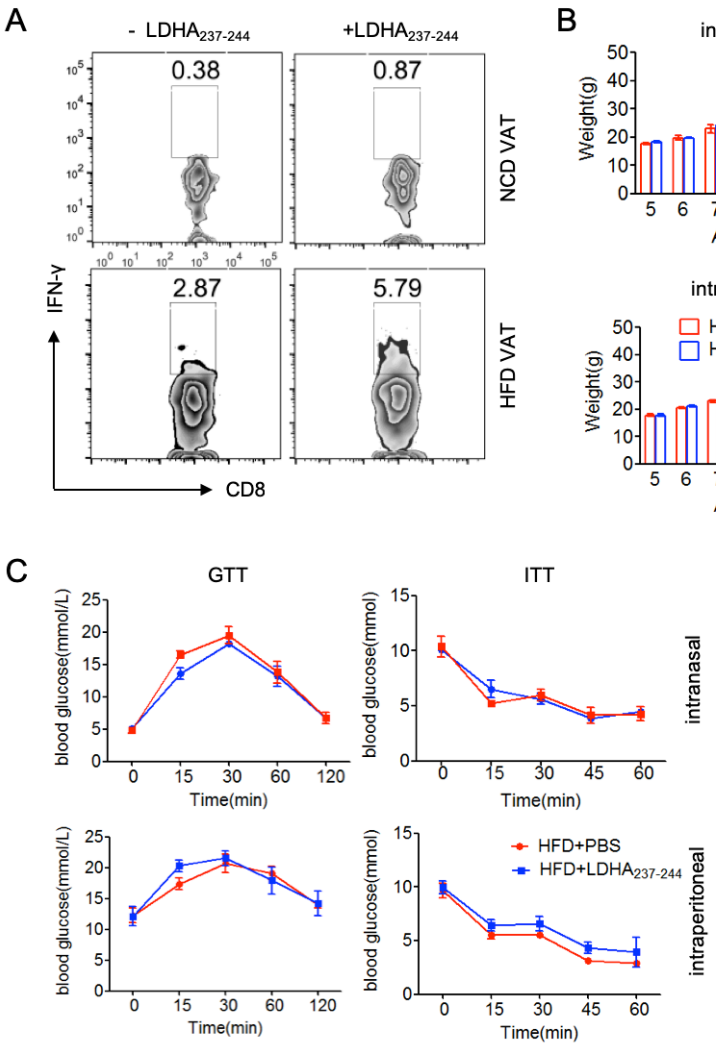

Figure S4. Intranasal or intraperitoneal administration of a single $LDHA_{237-244}$ peptide fails to affect the weight gain, glucose intolerance and insulin resistance in HFD-fed obese mice, Related to Figure 5

(A) Representative FACS indicating intracellular IFN-γ staining of VAT-infiltrated $CD8^+$ T cells stimulated with RMAS cells with RMAS cells loaded with or without $LDHA_{237-244}$ peptide.

(B) Comparison of changes in body weight between high-fat diet (HFD)-fed mice treated intranasally (upper) or intraperitoneally (lower) with $LDHA_{237-244}$ and PBS (n=4-5 mice per group). Error bars represent means ± SEM.

(C) Results of glucose tolerance (GTT) (i.p. 1 g per kg glucose, after 16 h fasting) and insulin tolerance (ITT) (i.p.,0.75 U insulin per kg body weight, after 3.5 h fasting) tests in HFD-fed mice treated intranasally (upper) or intraperitoneally (lower) with $LDHA_{237-244}$ and PBS (n =5 mice per group). Error bars represent means ± SEM. Data are representative of two experiments.

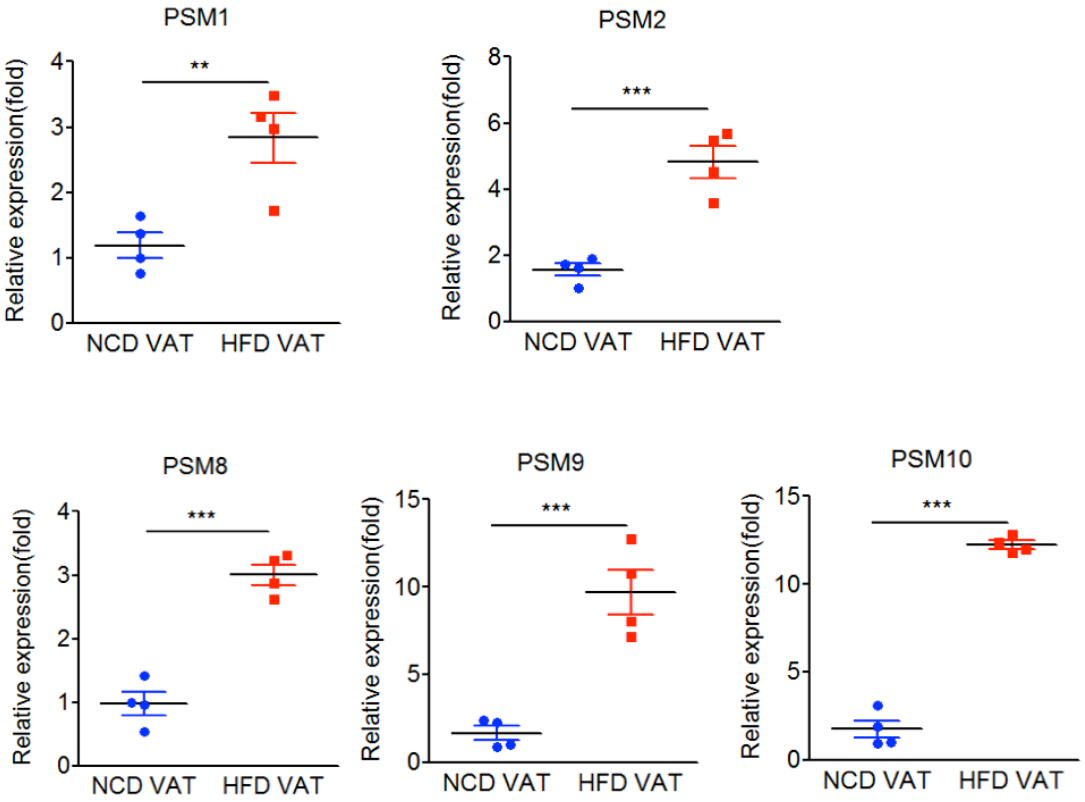

Figure S5. The mRNA expression of proteasomes (PSM1/2) and immunoproteasomes (PSM8/9/10) is increased in obese visceral adipose tissues, Related to Figure 6

Quantitative real-time PCR analysis of the mRNA expression of proteasomes (PSM1/2) and immunoproteasomes (PSM8/9/10) catalytic subunits in the epididymal fat pads from mice after 4-week NCD or HFD feeding (4 mice per group) Data are means and error bars are ±SEM.

* $p < 0.05$, ** $p < 0.01$,and *** $p<0.0001$, determined by Student's t-test.

Table S3. The exclusive high confidence H2-Kb-bound peptides from visceral adipose tissues of HFD-fed mice, Related to Figure 2

HFD VAT-exclusive MIP	Sequence	Length	Charge	MH+ [Da]	ΔM [ppm]	RT [min]	Proteins	Protein Accessions	Mascot IonScore	Sequest q-Value	MHC binding Affinity (IC_{50} nM)
1.	AALIYTSV	8	1	837.4681	-4.22	32	2	Q6PDL0,Q8R1Q8	31		67.9
2.	AAVKFHNL	8	2	899.5085	-1.48	13.39	1	Q64521	26		15.8
3.	AAYEFTTL	8	1	915.4449	-1.06	36.61	1	P32233	25		3.3
4.	ANVQYMRV	8	2	980.496	-2.34	18.99	1	Q61805	34		31.8
5.	ASTIAYLAL	9	2	922.5235	-1.04	28.57	1	O70503	28		252.5
6.	ASVVFNQL	8	2	877.477	-0.9	18.86	1	Q64288	25		10.9
7.	ATLRYASL	8	2	894.5022	-2.45	21.8	1	Q9DBR4	23		3.9
8.	DFFNYAGL	8	1	946.4321	1.68	33.05	1	P12265	27		43.4
9.	FAASYSAL	8	1	829.4089	-0.24	28.48	1	Q8BFW3	22		81.8
10.	GQYEFHSL	8	2	980.4457	-1.55	23.22	1	Q61805	33		91.9
11.	IGPYFEHNM	9	2	1107.491	-1.53	25.46	1	Q8VCB3	24		60.6
12.	ISDVRVTQL	9	2	1030.586	-3.22	31.18	1	P55065	22		355.6
13.	KSYDMSQV	8	2	957.4305	-4.36	27.95	1	Q8C8J0	21		199.4
14.	KSYLMNKL	8	2	996.5522	-2.54	17.72	3	Q01514,Q8CFB4, Q9Z0E6	28		29.4
15.	KVYTFNSV	8	2	957.5032	-0.91	21.38	3	G5E829,Q6Q477, Q9R0K7	27		10.5
16.	LAAQFSQL	8	2	877.477	-0.9	18.86	1	Q9DCB4	31		62
17.	LAPVYQRL	8	2	959.5665	-0.89	22.4	1	P82198	26		17.7
18.	NSFRYNGL	8	2	970.4738	-0.34	21.83	1	P41105	21		9.3
19.	QNYTYSSL	8	1	975.4399	-1.91	26.3	1	Q810S1	21		3.9

20.	RSYDFEFM	8	2	1094.459	-1.76	35.43	1	P40336	21		21.5
21.	SAPQFSKL	8	2	877.4777	-0.21	18.92	1	Q8K007	28		13.9
22.	SAPQYSRL	8	2	921.4781	-0.88	14.1	1	Q8CFG0	24		8.1
23.	SAYQRGESL	9	2	1010.488	-2.32	12.24	1	O35382	26		233.2
24.	SGLKYVNV	8	2	879.4932	-0.3	20.85	1	Q8VCP8	26		14.6
25.	SGLVYKNV	8	2	879.4922	-1.47	20.64	1	Q80TI1	26		30.4
26.	SGNIFVASL	9	2	907.4867	-1.83	27.44	1	O88495	25		35.8
27.	SIVSYNHL	8	2	932.4822	-1.5	22.3	1	Q9JHU9	21		10.2
28.	SNPEFRQL	8	2	990.4994	-0.99	18.61	1	Q3UWM4	27		17.3
29.	SSGDFPSL	8	1	809.3663	-1.58	32.32	1	Q9WVK4	24		138.2
30.	SSYNYRVV	8	2	987.4875	-1.98	18.4	1	P11881	26		5.4
31.	STFSFTKV	8	2	916.4765	-1.09	25.63	1	Q3TZZ7	21		7.7
32.	TTYKYEMI	8	2	1048.502	-0.21	24.58	1	Q8QZY1	28		28.6
33.	VFTEVANL	8	1	892.4758	-1.94	34.23	1	Q62141	22		195.2
34.	VFYEREVQM	9	2	1200.569	-2.64	25.49	1	Q80SY3	31		86.2
35.	VGINYREV	8	2	949.5077	-2.65	20.47	1	Q01320	22		46.2
36.	VNFEFPEF	8	2	1028.47	-1.98	50.37	1	P62082	22		43.3
37.	VNILENYL	8	2	977.5284	-1.93	31.24	1	Q64435	22		402.5
38.	VNIQYEVI	8	2	977.5284	-1.93	31.24	1	Q60961	25		324.5
39.	VNIQYLDL	8	2	977.529	-1.24	31.14	1	Q8R0G9	21		17
40.	AIYAFSHL	8	2	921.482	-1	30.93	1	Q9JJ59		0	2.2
41.	GTYDYTQL	8	1	960.4302	-0.77	30.12	1	Q8K2A8		0	31.7
42.	RAPVYARI	8	2	945.5602	-2.83	13.58	1	P52840		0	25
43.	RAYLFAHV	8	2	976.5349	-1.48	22.42	1	Q5SWD9		0	2.5
44.	RVYEFTRA	8	2	1041.546	-1.74	13.38	1	Q8VI38		0.049	45.2
45.	SGYDYYHV	8	2	1003.415	-0.8	22.78	1	O08785		0	6.9

46.	SQYRFEHL	8	2	1079.525	-1.46	17.98	1	Q3UJK4		0	3.8
47.	SSPKFSEI	8	2	894.4559	-1.01	18.91	1	Q91VM3		0	53.5
48.	AAYGFRNI	8	2	911.4717	-1.91	23.04	1	Q9CYQ7	30	0	9.6
49.	IGPRYSSV	8	2	878.4706	-2.85	15.19	1	Q5PRF0	26	0	19.4
50.	SAPLYTNL	8	1	878.46	-2.13	31	1	Q8K4S1	25	0	4.6
51.	SAYEVIKL	8	2	922.5235	-1.04	28.57	2	P06151,P16125	38	0	56.8
52.	STFVYNTM	8	1	962.4263	-2.65	29.89	1	Q8CFB4	38	0	7.7
53.	**SAYEFYHA**	**8**	**2**	**987.4195**	**-1.22**	**22.43**	**1**	**P97481**	**26**		**13**
54.	**SGTQYFRV**	**8**	**2**	**957.477**	**-1.99**	**19.42**	**1**	**P97412**	**21**		**201.2**
55.	**SLYQPAGL**	**8**	**1**	**848.4503**	**-1.12**	**31**	**1**	**P19096**	**40**		**70.7**
56.	**SSPHYTTL**	**8**	**2**	**905.4344**	**-2.16**	**14.13**	**1**	**P27046**		**0**	**12.2**
57.	**STTVFHSL**	**8**	**2**	**891.4551**	**-2.26**	**21.06**	**1**	**P19096**		**0**	**44.2**

Note: five of the peptides highlighted in red color did not display HFD VAT MIP specificity at the source protein level.

Table S4. Peptides and their potential source proteins found to be exclusively expressed in VAT MIP from HFD-induced obese mice as described in Section 2, Related to Figure 2

Peptide			Source Protein		
Sequence	Length	Affinity(nM)	Accession No	Name	Peptide Position
				Proteins involved in Glucose metabolism	
AAVKFHNL	8	15.8	Q64521	Glycerol-3-phosphate dehydrogenase 2	450-457
DFFNYAGL	8	43.4	P12265	Beta-glucuronidase	206-213
IGPYFEHNM	9	60.6	Q8VCB3	Glycogen synthase 2	66-74
SAYEVIKL	8	56.8	P06151	L-lactate dehydrogenase A chain	237-244
			P16125	L-lactate dehydrogenase B chain	238-245
				Proteins involved in lipid metabolic process	
ASTIAYLAL	9	252.5	O70503	17-beta-hydroxysteroid dehydrogenase 12	16-24
ISDVRVTQL	9	355.6	P55065	Phospholipid transfer protein	65-73
RAPVYARI	8	25	P52840	Sulfotransferase 1A1	68-75
RVYEFTRA	8	45.2	Q8VI38	Forssman glycolipid synthase	271-278
SAPLYTNL	8	4.6	Q8K4S1	Phosphoinositide phospholipase C-epsilon-1	1232-1239
SIVSYNHL	8	10.2	Q9JHU9	Inositol-3-phosphate synthase 1	328-335
STFSFTKV	8	7.7	Q3TZZ7	Extended synaptotagmin-2	157-164
				Proteins involved in protein metabolism	
AAYEFTTL	8	3.3	P32233	Developmentally-regulated GTP-binding protein 1	92-99
NSFRYNGL	8	9.3	P41105	60S ribosomal protein L28	36-43
SNPEFRQL	8	17.3	Q3UWM4	Lysine-specific demethylase 7A	775-782
SQYRFEHL	8	3.8	Q3UJK4	GTP-binding protein 2 (GTP-binding-like protein 2)	78-85
SSPKFSEI	8	53.5	Q91VM3	WD repeat domain phosphoinositide-interacting protein 4	70-77
TTYKYEMI	8	28.6	Q8QZY1	Eukaryotic translation initiation factor 3 subunit L	353-360

VFTEVANL	8	195.2	Q62141	Paired amphipathic helix protein Sin3b	205-212
VNFEFPEF	8	43.3	P62082	40S ribosomal protein S7	185-192
				Proteins involved in establishment of localization	
AIYAFSHL	8	2.2	Q9JJ59	ATP-binding cassette sub-family B member 9	23-30
IGPRYSSV	8	19.4	Q5PRF0	HEAT repeat-containing protein 5A	1980-1987
			Q6Q477	Plasma membrane calcium-transporting ATPase 4	565-572
KVYTFNSV	8	10.5	Q9R0K7	Plasma membrane calcium-transporting ATPase 2	553-560
			G5E829	Plasma membrane calcium-transporting ATPase 1	574-581
LAPVYQRL	8	17.7	P82198	Transforming growth factor-beta-induced protein ig-h3	670-677
QNYTYSSL	8	3.9	Q810S1	Calcium uniporter regulatory subunit MCUb	281-288
RSYDFEFM	8	21.5	P40336	Vacuolar protein sorting-associated protein 26A	105-112
VFYEREVQM	9	86.2	Q80SY3	V-type proton ATPase subunit d 2	292-300
VNIQYLDL	8	17	Q8R0G9	Nuclear pore complex protein Nup133	337-344
				Proteins involved in response to stimulus	
AALIYTSV	8	67.9	Q6PDL0	Cytoplasmic dynein 1 light intermediate chain 2	267-274
			Q8R1Q8	Cytoplasmic dynein 1 light intermediate chain 1	280-287
ANVQYMRV	8	31.8	Q61805	Lipopolysaccharide-binding protein	474-481
GQYEFHSL	8	91.9			74-81
ASVVFNQL	8	10.9	Q64288	Olfactory marker protein	156-163
ATLRYASL	8	3.9	Q9DBR4	Amyloid-beta A4 precursor protein-binding family B member 2	387-394
FAASYSAL	8	81.8	Q8BFW3	Protein phosphatase 1 regulatory subunit 15B	93-100
KSYLMNKL	8	29.4	Q8CFB4	Guanylate-binding protein 5	51-58
STFVYNTM	8	7.7			124-131
LAAQFSQL	8	62	Q9DCB4	cAMP-regulated phosphoprotein 21	547-554
SAPQFSKL	8	13.9	Q8K007	Extracellular sulfatase Sulf-1	230-237
SAPQYSRL	8	8.1	Q8CFG0	Extracellular sulfatase Sulf-2	231-238

SAYQRGESL	9	233.2	O35382	Exocyst complex component 4	322-330
SGNIFVASL	9	35.8	O88495	G protein-coupled receptor 50	70-78
SGYDYYHV	8	6.9	O08785	Circadian locomoter output cycles protein kaput	308-315
SSGDFPSL	8	138.2	Q9WVK4	EH domain-containing protein 1	349-356
SSYNYRVV	8	5.4	P11881	Inositol 1,4,5-trisphosphate receptor type 1	1169-1176
VGINYREV	8	46.2	Q01320	DNA topoisomerase 2-alpha	67-74
VNILENYL	8	402.5	Q64435	UDP-glucuronosyltransferase 1-6	214-221
				Others	
AAYGFRNI	8	9.6	Q9CYQ7	Nuclear prelamin A recognition factor	351-358
GTYDYTQL	8	31.7	Q8K2A8	Dol-P-Man:Man(5)GlcNAc(2)-PP-Dol alpha-1,3-mannosyltransferase	84-91
KSYDMSQV	8	199.4	Q8C8J0	Sperm-tail PG-rich repeat-containing protein 2	431-438
RAYLFAHV	8	2.5	Q5SWD9	Pre-rRNA-processing protein TSR1 homolog	250-257
SGLKYVNV	8	14.6	Q8VCP8	Adenylate kinase isoenzyme 6	27-34
SGLVYKNV	8	30.4	Q80TI1	Pleckstrin homology domain-containing family H member 1	460-467
VNIQYEVI	8	324.5	Q60961	Lysosomal-associated transmembrane protein 4A	60-67

Note: peptides sequence, length, predicted H2-Kb-binding affinity (IC_{50}), protein name, accession number and function, according to Uniprot database are listed.

Table S5. Several known obesity-associated proteins are detected in the obese VAT-exclusive MIPs source proteome, Related to Figure 2

Protein ID	Protein name (gene)	Functions	Obesity-association	References
Q61805	Lipopolysaccharide-binding protein (Lbp)	Lipid binding	LBP is an inflammatory marker associated with obesity-related insulin resistance	(Kim et al., 2016; Moreno-Navarrete et al., 2012)
O88495	Melatonin-related receptor (Gpr50)	G-protein coupled receptor activity; regulating energy metabolism	GPR50 knockout mice were partially resistant to diet-induced obesity.	(Ivanova et al., 2008).
P55065	Phospholipid transfer protein (Pltp)	lipid transporter activity	PLTP mass and activity have been found to be elevated in the plasma of type 2 diabetes mellitus (T2DM) and obese patients. PLTP mass and activity have been found to be positively associated with BMI, fat mass and leptin levels. PLTP activity is independently associated with nonalcoholic fatty liver disease.	(Qin et al., 2014) (Tzotzas et al., 2009)
Q8VCB3	Glycogen synthase 2 (Gys2)	Glucose binding	GYS2 as a novel genetic factor for polycystic ovary syndrome through obesity-related condition.	(Hwang et al., 2012)

Q8CFG0	Extracellular sulfatase Sulf-2 (Sulf2)	arylsulfatase activity	SULF2 strongly predisposes to fasting and postprandial triglycerides in patients with obesity and type 2 diabetes mellitus.	(Hassing et al., 2014)
P06151	L-lactate dehydrogenase A chain (Ldha)	pyruvate fermentation to lactate	Lactate dehydrogenase gene is downregulated in visceral white adipose tissue of HFD-fed rats, suggesting a decreased anaerobic degradation of glucose in adipose tissue. As a result, pyruvate would be directed to acetyl-CoA production, which in turn would fuel fatty acid biosynthesis and triglyceride storage. However, it has also been reported that activating or overexpressing LDH-A react against lipid accumulation by deviating pyruvate to lactate. Lactate increases the destiny of white adipose cells towards a brown phenotype. The elevated level of LDHA has been suggested to be related with the reduction of body weight gain.	(Lopez et al., 2004; Parray and Yun, 2015)
Q64521	Glycerol-3-phosphate dehydrogenase 2, mitochondrial (Gpd2)	Calcium ion binding; gluconeogenesis; NADH metabolic process	Mitochondrial glycerol 3-phosphate dehydrogenase (mGPDH) is an integral component of the respiratory chain. Lou/C, a rat strain derived from Wistar, is resistant to age- and diet-related obesity, and this feature has been shown to be linked to a high expression and activity of mitochondrial glycerol-3-phosphate dehydrogenase. Deficiency of the mitochondrial glycerol 3-phosphate dehydrogenase contributes to hepatic steatosis.	(Taleux et al., 2009) (Zheng et al., 2019)

Table S6. Selected potential candidate peptides for immunogenicity evaluation, Related to Figure 3 and Figure 4

Group	Name	Source protein	Protein_ID	Function	Sequence	IC50(nM)	HFD-VAT MIP	NCD-VAT MIP
G1	DHB_{16-24}	17-beta-hydroxys-teroid dehydrogenase 12	O70503	Oxidoreductase; lipid metabolism	ATLRYASL	252.2	+	-
	LBP_{74-81}	Lipopolysaccharide-binding protein	Q61805	Lipid binding; immune system process; response to stimulus	GQYEFHSL	91.9	+	-
	$LDHA_{237-244}$	L-lactate dehydrogenase A or B chain	P06151	Oxidoreductase; glucose metabolism; response to stimulus	SAYEVIKL	56.8	+	-
	$APBB2_{387-394}$	Amyloid-beta A4 precursor protein-binding family B member 2	Q9DBR4	Nucleic acid-templated transcription; response to stimulus	ATLRYASL	3.9	+	-
	$V\text{-}ATPase_{292-300}$	V-type proton ATPase subunit d 2	Q80SY3	Hydrolase	VFYEREVQM	86.2	+	-

G2	ITPR1$_{1169-1176}$	Inositol 1,4,5-trisphosphate receptor type 1	P11881	Calcium ion transport	SSYNYRVV	5.4	+	-
	EXOC4$_{322-330}$	Exocyst complex component 4	O35382	Golgi to plasma membrane transport	SAYQRGESL	233.2	+	-
	GBP5$_{124-131}$	Guanylate-binding protein 5	Q8CFB4	GTPase activity	STFVYNTM	7.7	+	-
	AK6$_{10-17}$	Adenylate kinase isoenzyme 6	Q8VCP8	ATPase activity	SGLKYVNV	14.6	+	-
	EHD1$_{349-356}$	EH domain-containing protein 1	Q9WVK4	ATP/GTP binding; calcium ion binding	SSGDFPSL	138.2	+	-
G3	CATA$_{384-392}$	Catalase	P24270	Cholesterol metabolic process	ANYQRDGPM	214.7	+++	+
	PLIN2$_{213-221}$	Perilipin-2	P43883	Lipid storage; long-chain fatty acid transport	SNYERLESL	64.4	+++	+
	D19L3$_{433-440}$	Probable C-mannosyltransferase DPY19L3	Q71B07	Transferase activity	SVVAFHNL	8.69	+++++++	+

Note: a plus or multiple plus indicates the abundance of the indicated peptide in the given tissue-derived MIP; the minus sign indicates that the indicated peptide cannot be detected in the given tissue-derived MIP.

Transparent Methods

Animal models

Four-week-old male C57BL/6J wild-type mice (HFK Bioscience, Beijing, China) were maintained under a 12 h light-dark cycle in specific pathogen-free facilities, and were allowed free access to sterilized water and to either a high fat diet (HFD, D12492, 60 Kcal% fat, Research Diets) or a normal chow diet (NCD, D12450B 10 Kcal% fat, Research Diets). For the glucose tolerance test (GTT), the mice were made to fast for 16 h prior to intraperitoneal administration of glucose (1g kg^{-1}). Blood glucose was measured from tail vein at indicated time points with a glucometer (ONETOUCH Ultra). For the insulin tolerance test (ITT), mice were made to fast for 4 h prior to intraperitoneal administration of insulin (Novolin; 0.75U kg^{-1}) and blood glucose concentrations were measured at indicated time points. All procedures were approved by the Institute Animal Care and Use Committee of the Third Military Medical University (Chongqing, China).

Isolation of MIP from VAT

The epididymal fat pad (VAT samples) (total 28 g) were collected from 25 HFD-fed obese male mice or 75 NCD-fed lean male mice at 12 weeks of age from three different batches, respectively, and immediately lysed in 40 ml of ice-cold lysis buffer (50 mM Tris-HCl, 150 mM NaCl, and 1% of CHAPS, pH 8.0) containing “complete” protease inhibitor (Roche). Cell lysates were clarified by several rounds of centrifugation (12000g, 30 min, 4°C), and the supernatant was collected and used for immunoaffinity chromatography. The MIPs were isolated following a method described previously (Delgado et al., 2009; Escobar et al., 2008; Purcell, 2004) with some modifications. Initially, immunoaffinity columns were constructed

based on the following steps: 1) the top-cap of 1 ml HiTrap NHS-activated HP column (Code No:17-0716-01, GE Healthcare) was removed and a drop of ice-cold 1 mM HCl was introduced into the top to avoid air bubble formation; 2) 3 × 2 ml ice-cold 1 mM HCl was injected to wash out the isopropanol in the column at a flow rate not exceeding 1 ml/min. 3) For antibody coupling, 10 ml of 1 mg/ml anti-H2-Kb mAb (clone: Y-3, Bioxcell company) antibody in coupling buffer (0.2 M NaHCO3, 0.5 M NaCl, pH 8.3) was passed through the column repeatedly at a flow rate of 1 ml/min for 4 h at 4 °C. 4) To deactivate any excess active groups that had not coupled to the ligand and to wash out the non-specifically bound ligands, 3 × 2 ml of Buffer A (0.5 M ethanolamine, 0.5 M NaCl, pH 8.3) and 3 × 2 ml of Buffer B (0.1 M sodium acetate, 0.5 M NaCl, pH 4) were injected into the column alternately; after the columns were maintained at room temperature for 15–30 min, 3 × 2 ml of Buffer B and 3 × 2 ml of Buffer A were injected into the column alternately; 15 ml of lysis buffer (50 mM Tris-HCl, pH 8.0 150 mM NaCl and 1% of CHAPS) was injected into the column. Next, the VAT proteolytic solution was repeatedly circulated in the column overnight at a flow rate of 1 ml/min at 4°C. Following this, the column was washed with several buffers in the following order: 15 ml of wash buffer 1 (50 mM Tris-HCl, pH 8.0, 150 mM NaCl, and 1% of CHAPS), 15 ml of wash buffer 2 (50 mM Tris-HCl, pH 8.0, 150 mM NaCl in deionized H_2O), 25 ml of wash buffer 3 (50 mM Tris-HCl, pH 8.0, 450 mM NaCl in deionized H_2O), and 35 ml of wash buffer 4 (50 mM Tris-HCl, pH 8.0, in deionized H_2O). Subsequently, the HLA-peptide complexes were eluted with 6 ml of 10% acetic acid. The ultrafiltration filters (3.0-kDa cutoff Microcon, Millipore) were prewashed with 0.1 N acetic acid and 10% acetonitrile to remove contaminants interfering with the mass spectrometry, and the mixture of peptides and class I heavy-chain and β2-microglobulin were

separated by ultrafiltration at 10000 × g (Escobar et al., 2008; Murphy et al., 2017). After ultrafiltration, the peptides mixtures were desalinated and concentrated by Micro-Tip reversed-phase C18 columns (Merck) (Bassani-Sternberg et al., 2010). The C18 columns were washed with 80% acetonitrile in 0.1% TFA, equilibrated with 0.1% TFA, and loaded with the peptide mixture. The C18 columns were washed additionally by 0.1% TFA. Lastly, the peptides were eluted with 400 μl 80% acetonitrile in 0.1% TFA, and all peptide elutions were vacuum concentrated to a final volume of 20 μl prior to mass spectrometry analysis.

MIP analysis using LC-MS/MS

MIP samples were loaded into an analytical column (Acclaim™ PepMap™ 100, 75 μm ×15 cm, C18, 3 μm, 100 Å, Thermo Fisher Scientific) with a Trap Column (Acclaim™ PepMap™ 100, 75 μm×2 cm, C18, 3 μm, 100 Å, Thermo Fisher Scientific) and separated by reversed-phase chromatography (Easy nanoLC1000, Thermo Fisher Scientific) using a 120 min gradient at a flow rate of 300 nL/min. The gradient was composed of Solvent A (0.1% formic acid in water) and Solvent B (0.1% formic acid in acetonitrile); the elution gradient was as follows: 2-7% B in 3 min, 7-22% B in 96 min, 22-35% B in 10 min, 35-90% B in 2 min, 90% B for 5 min and 90-2% B in 2 min, 2% B for 2 min. The eluted peptides were sprayed into the LTQ Orbitrap using nano-electron spray ionization (NSI) at a capillary voltage of 2.5 KV and 300 ℃capillary temperature. The instrument was operated in the data-dependent mode. Survey MS spectra from 350.0–1800.0 m/z were obtained in the orbitrap at 60,000 M/ΔM resolution, followed by data dependent acquisition (DDA) of the top 16 most abundant precursor ions with an isolation window of 2.0 m/z, and followed by MS/MS scans of the ion trap using product ion scans (relative CID energy 35) of the top 16 most abundant precursor ions in the survey scan. MS

scans were captured in profile mode, while the MS/MS scans was captured in centroid mode. The product ion scans were obtained using a 2.0-unit isolation width and normalized collision energy of 35 in an LTQ Orbitrap Velos Pro MS spectrometer (Thermo Fisher Scientific). Three replicate injections were performed for each set of samples.

Database search and spectral annotation

Acquired tandem mass spectrometric spectra were searched using Mascot (version 2.3, Matrix Science) and the Sequest HT search engine with the Proteome Discoverer software (PD) (version 1.4.0.288, Thermo Fisher Scientific) against the UniProt mouse FASTA protein database and reversed decoy sequences. MS/MS spectra were captured in CID mode. Mascot search parameters were set as follows: precursor ion mass tolerance 5 ppm, fragment ion mass tolerance 0.8Da, no enzyme specificity, oxidized methionine was allowed as a dynamic modification, FDR<5% (peptide-spectrum match level). Protein grouping was disabled, allowing multiple annotations of peptides (for example, conserved sequence mapping into multiple proteins). The Sequest HT used the same search parameters as Mascot. Mascot and Sequenst search results in technical triplicates were combined to establish datasets of HFD VAT MIP and NCD VAT MIP. Firstly, peptides with either an Ionscore>20 in Mascot search (Al-Shahib et al., 2010; Kowalewski and Stevanovic, 2013; Kumar et al., 2015; Ni et al., 2019) or a q-value<0.05 in Sequest search (Franchin et al., 2014; Kall et al., 2008) were collected. Secondly, peptide lengths were limited to 8-12 amino acids. Finally, high confidence H2-Kb-associated peptides were identified by IC_{50}<500 nM (NetMHC 4.0: http://www.cbs.dtu.dk/services/NetMHC/), (Andreatta and Nielsen, 2016)

Determination of MHC class I motifs

We used the weblogo program (http://weblogo.berkeley.edu/logo.cgi) to visualize the characteristics of the binding motifs. The information content at each position in the sequence motif corresponds to the height of a column of letters. The height of each letter within the column is proportional to the frequency of the corresponding amino acid at that position.

Annotation enrichment analysis and functional annotation of MIP source proteins

Biological annotation and KEGG pathway enrichment of the VAT MIP source proteins was performed using the R package “clusterProfiler” (version 3.10.1).Terms with adjusted P value < 0.01 were considered significant.

Peptide Synthesis

The peptides were synthesized at a purity>95% at the Chinese Peptide Company (Hangzhou, China). Synthetic peptides were used for validation of LC-MS/MS identification as well as for functional experiments.

H2-Kb binding assays

Peptide binding to H2-Kb was measured using the transporter associated with TAP-deficient RMAS cell line. Briefly, RMAS cells were cultured overnight in complete medium at 26 °C, 5% CO_2. The RMAS cells ($1x10^6$ cells/ml) were incubated with or without each peptide pool (total 100 μg/ml) for 3 h at 26 °C, followed by a second incubation for 3 h at 37 °C, 5% CO_2. An H2-Kb-binding LCMV peptide GP_{33-41} (KAVYNFATM) was used as a positive control. After incubation, the cells were washed twice with ice-cold PBS and stained with PE-conjugated anti-mouse H2-Kb mAb (eBioscience, AF6) for 30 min at 4 °C. The cells were washed and detected by flow cytometry (BD FACS Calibur). Data analysis was performed using the FlowJo software (v7.6.3, Treestar, San Carlos, CA, USA).

Amplification of Peptide-Specific $CD8^+$T Cells and intracellular cytokine staining

Splenocytes isolated from C57BL/6J mice were stimulated with each peptide pool or single peptide (100 μg/ml) in complete medium containing recombinant IL-2 (30 IU/ml; Roche), and half the medium was replaced with complete medium supplemented with IL-2 every 3–4 days. Cell cultures were restimulated with the peptide pool or single peptide (50 μg/ml)-pulsed RMAS cells or only RMAS cells on day 7. To block the H2-Kb-restricted recognition of $CD8^+$ T cells, anti-H2-Kb antibody Y-3 (10 μg/ml) was added to the cell cultures. The presence of peptide-specific $CD8^+$ T cells was assessed by intracellular IFN-γ and TNF-α staining. Two hours after the restimulation, 0.65μl ml^{-1}GolgiStop™ (BD Biosciences) was added into each culture at 37 °C and incubated for an additional 4 hours. Before staining, all cell preparations were incubated with anti-mouse CD16/32 (BD Biosciences) for 10 min on ice to block the Fc receptors. Dead cells were excluded from the analysis by using the fixable Viability Dye eFluor® 780 (eBioscience). Percp-cy5.5-conjugated CD3 mAb (clone:53-6.7 eBioscience) and FITC-conjugated anti-CD8α mAb (clone:17A2 eBioscience) were used to label cells for 30 min on ice. After washing with the flow cytometer buffer (PBS/1% FBS), cells were fixed and then labeled with PE-conjugated anti-mouse TNF-α (clone: MP6-XT22 eBioscience) or APC-conjugated anti-mouse IFN-γ (clone: XMG1.2 eBioscience) at 4 °C in a permeabilization buffer. PE or APC-conjugated isotype IgG1 was used as a negative staining control (eBioscience). Flow cytometry data were acquired for each of the experiments using a BD FACS Calibur (BD Biosciences, Franklin Lakes, NJ). Data analysis was performed using the FlowJo software.

Pentamer staining

Lymphocytes were isolated from the mesenteric lymph nodes of HFD-fed obese mice and NCD-fed lean mice post the 8-week feeding. A single cell suspension was prepared in PBS at a cell concentration of 1-2·10^6 cells/100 μl, initially stained with Fixable Viability Dye eFluor® 780 (eBioscience) and washed, and then stained with PE-conjugated pentamers (Proimmune,5 μl/test) for 15 min-incubation at 37 ºC in dark. After washing twice with FACS buffer, cells were incubated with FITC-conjugated-anti-mouse CD8 (clone: 17A2, eBioscience) at 4 ºC for 30 min. Cells were washed twice with FACS buffer, and fixed with 1% polyformaldehyde. After washing, stained cells were resuspended in 200-300 μl FACS buffer and measured using a BD FACS Calibur (BD Biosciences, Franklin Lakes, NJ).

Preparation of VAT-isolated stromal-vascular fractions (SVF)

Acquired epididymal VAT from HFD-fed obese mice and NCD-fed lean mice were divided into fine pieces in a weight boat containing 3 ml DPBS supplemented with 0.5% BSA. The VAT samples were then poured into 50 ml conical tubes, rinsed with 3 ml collagenase II digest solution consisting of 1X DPBS supplemented with 0.5% BSA, 10 mM CaCl2, and 4 mg/ml type II collagenase, and incubated in a rotational shaker (200 rpm, 37 ºC, 20 min). The VAT homogenate, along with 10 ml DPBS (0.5% BSA), was passed through a 100 μm filter into fresh 50 ml conical tubes. The VAT-isolated SVFs were obtained after centrifuging cell suspensions (500g, 4 ºC, 10 min) and discarding the supernatant. The VAT-isolated SVFs were restimulated with peptide (10 μg/ml)-pulsed RMAS cells or RMAS cells alone. The presence of peptide-specific $CD8^+$ T cells was assessed by intracellular IFN-γ and TNF-α staining.

Treatment of mice

C57BL/6J male mice administered HFD starting at 4 weeks of age were randomly divided into 4 groups (4-5 mice per group), two of which were administered 20 μg $LDHA_{237-244}$ peptide or PBS (once a day at day 1-5, 8, then once a week until the age of 12 weeks) intranasally, starting at 4 weeks of age, and the other two groups were injected intraperitoneally with 50 μg $LDHA_{237-244}$ peptide (twice a week for the first two weeks and once a week until the age of 12 weeks) or PBS simultaneously. Weight changes were monitored weekly until 12 weeks of age. GTT and ITT were measured at 12 weeks of age.

RNA Isolation and Quantitative Real-Time PCR

For real-time PCR, total RNA was extracted from 0.2 mg VAT using HiPure Universal RNA Kit(Magen company, Guangzhou, China). Real-time quantitative PCR was performed using TB Green™ Premix Ex Taq™ II (Tli RNaseH Plus) (Takara, Kyoto, Japan) for H2-Kb and TaqMan™ Gene Expression Master Mix (Applied Biosystems™, Foster City, CA, USA) for the other genes according to the manufacturer's instructions. The following primers were used: *H2-kb* (Fwd: ggctggtgaagcagagagac, Rev: cagcacctcagggtgacttt), *Ldha* (Mm01612132_g1, Thermo fisher), *Psmb1* (Mm00650840_m1, Thermo fisher), *Psmb2* (Mm00449477_m1, Thermo fisher), *Psmb8* (Mm00479004, Thermo fisher), *Psmb9* (Mm00440207, Thermo fisher), and *Psmb10* (Mm00479052_g1, Thermo fisher). Each sample run was performed in triplicate, and the relative mRNA expression levels were determined using the 2(-Delta Ct) method with *Gapdh* as the internal reference control.

Western bolt analysis

VAT from obese and lean mice were lysed in RIPA buffer (50 mM Tris-HCl pH 7.4, 1% Nonidet P-40,0.25% Na-deoxycholate, 150 mM NaCl, 1 mM EDTA) containing complete protease

inhibitor mixture (Roche Life Sciences), 1 mM Na3VO4 pH 9, 5 mM NaF, and 10 mM NEM (Sigma-Aldrich). H2-Kb molecules were separated from elution fractions using ultrafiltration with a 3-KDa cutoff. Samples were separated by SDS-PAGE and immunoblotted with the following primary antibodies: Rabbit polyclonal to MHC Class I H2-Kb (ab93364, Abcam), Rabbit monoclonal to mouse LDHA (ab101562, Abcam), and anti-mouse GAPDH antibody (ab181602, Abcam). After incubation with peroxidase-coupled secondary antibodies for 60 min, the immunocomplexes were visualized using a chemiluminescence reagent (Amersham, Freiburg, Germany), and the autoradiographs were scanned by an imaging densitometer.

Measurement of lactate dehydrogenase (LDH) activity

Total LDH activity in VAT was determined using the LDH activity assay kit (MAK06, Sigma) according to the manufacturer's protocol. Briefly, fresh VAT samples (100 mg) from HFD or NCD-fed mice were homogenized rapidly on ice in 500 μl of cold LDH Assay buffer and centrifuged at 10,000 g for 15 min at 4 °C to remove any insoluble materials; the soluble fraction was used for the assay. Changes in absorbance were determined by total LDH activity at 450 nm using BIO-RAD IMark™ Microplate Reader.

Immunoprecipitation and western blot analysis of ubiquitination

Pooled VAT tissues (0.5mg) from three or four obese or lean mice were washed twice with ice-cold PBS and lysed in 2 ml Triton-lysis buffer (20 mM Tris-HCl, pH 7.5, 150 mM NaCl, 5 mM EDTA, 2 mM dithiothreitol, 1%Triton X-100, 1% protease inhibitor cocktail, 1 mM PMSF) in the presence or absence of 10 μM MG132 (a proteasome inhibitor). The lysates were centrifuged at 12,000 × g for 10 min at 4 °C and the supernatant was precleared with 20 μL Protein A/G PLUS-Magnetic Beads (Thermo fisher) for 1 h at 4 °C. The lysates were

immunoprecipitated overnight with LDHA-specific rabbit polyclonal antibody (19987-1-AP, proteintech, 2 μg/test) at 4 °C, followed by incubation with protein A/G Magnetic Beads. This was followed by four washes with ice-cold lysis buffer and elution in 2X SDS sample buffer. The immunoprecipitates were boiled in 2X SDS sample buffer, resolved by SDS-PAGE, and subjected to overnight immunoblotting with specific antibodies against Lys48-specific Ubiquitin (clone: Apu2, Millipore, 1:1000) or LDHA (clone: EPR1563Y, Abcam, 1:1000) at 4 °C. Proteins were visualized using a goat anti-rabbit secondary antibody conjugated to HRP (D110058-0100, shanghai shengong company, 1:5000, 1 hour at room temperature) and a chemiluminescence detection system.

Statistical analysis

We used the Prism5 software (GraphPad Software) for all statistical tests. The unpaired two-group comparison was conducted using Student's t-test. Data were presented as the mean ± SD. $P<0.05$ (*), $P<0.01$ (**) and $P<0.001$(***) were considered statistically significant.

References:

Al-Shahib, A., Misra, R., Ahmod, N., Fang, M., Shah, H., and Gharbia, S. (2010). Coherent pipeline for biomarker discovery using mass spectrometry and bioinformatics. BMC Bioinformatics *11*, 437.

Andreatta, M., and Nielsen, M. (2016). Gapped sequence alignment using artificial neural networks: application to the MHC class I system. Bioinformatics *32*, 511-517.

Bassani-Sternberg, M., Barnea, E., Beer, I., Avivi, I., Katz, T., and Admon, A. (2010). Soluble plasma HLA peptidome as a potential source for cancer biomarkers. Proc Natl Acad Sci U S A *107*, 18769-18776.

Delgado, J.C., Escobar, H., Crockett, D.K., Reyes-Vargas, E., and Jensen, P.E. (2009). Identification of naturally processed ligands in the C57BL/6 mouse using large-scale mass spectrometric peptide sequencing and bioinformatics prediction. Immunogenetics *61*, 241-246.

Escobar, H., Crockett, D.K., Reyes-Vargas, E., Baena, A., Rockwood, A.L., Jensen, P.E., and Delgado, J.C. (2008). Large scale mass spectrometric profiling of peptides eluted from HLA molecules reveals N-terminal-extended peptide motifs. J Immunol *181*, 4874-4882.

Franchin, C., Pivato, M., Rattazzi, M., Arrigoni, G., and Millioni, R. (2014). OFFGEL fractionation of peptides: where really is your sample? J Chromatogr A *1355*, 278-283.

Hassing, H.C., Surendran, R.P., Derudas, B., Verrijken, A., Francque, S.M., Mooij, H.L., Bernelot Moens, S.J., Hart, L.M., Nijpels, G., Dekker, J.M., et al. (2014). SULF2 strongly prediposes to fasting and postprandial triglycerides in patients with obesity and type 2 diabetes mellitus. Obesity *22*, 1309-1316.

Hwang, J.Y., Lee, E.J., Jin Go, M., Sung, Y.A., Lee, H.J., Heon Kwak, S., Jang, H.C., Soo Park, K., Lee, H.J., Byul Jang, H., et al. (2012). Genome-wide association study identifies GYS2 as a novel genetic factor for polycystic ovary syndrome through obesity-related condition. Journal of human genetics *57*, 660-664.

Ivanova, E.A., Bechtold, D.A., Dupre, S.M., Brennand, J., Barrett, P., Luckman, S.M., and Loudon, A.S. (2008). Altered metabolism in the melatonin-related receptor (GPR50) knockout mouse. American journal of physiology. Endocrinology and metabolism *294*, E176-182.

Kall, L., Storey, J.D., MacCoss, M.J., and Noble, W.S. (2008). Posterior error probabilities and false discovery rates: two sides of the same coin. J Proteome Res *7*, 40-44.

Kim, K.E., Cho, Y.S., Baek, K.S., Li, L., Baek, K.H., Kim, J.H., Kim, H.S., and Sheen, Y.H. (2016). Lipopolysaccharide-binding protein plasma levels as a biomarker of obesity-related insulin resistance in adolescents. Korean journal of pediatrics *59*, 231-238.

Kowalewski, D.J., and Stevanovic, S. (2013). Biochemical large-scale identification of MHC class I ligands. Methods Mol Biol *960*, 145-157.

Kumar, G., Gotesman, M., and El-Matbouli, M. (2015). Interaction of Tetracapsuloides bryosalmonae, the causative agent of proliferative kidney disease, with host proteins in the kidney of Salmo trutta. Parasitol Res *114*, 1721-1727.

Lopez, I.P., Milagro, F.I., Marti, A., Moreno-Aliaga, M.J., Martinez, J.A., and De Miguel, C. (2004). Gene expression changes in rat white adipose tissue after a high-fat diet determined by differential display. Biochemical and biophysical research communications *318*, 234-239.

Moreno-Navarrete, J.M., Ortega, F., Serino, M., Luche, E., Waget, A., Pardo, G., Salvador, J., Ricart, W., Fruhbeck, G., Burcelin, R., et al. (2012). Circulating lipopolysaccharide-binding protein (LBP) as a marker of obesity-related insulin resistance. International journal of obesity *36*, 1442-1449.

Murphy, J.P., Konda, P., Kowalewski, D.J., Schuster, H., Clements, D., Kim, Y., Cohen, A.M., Sharif, T., Nielsen, M., Stevanovic, S., et al. (2017). MHC-I Ligand Discovery Using Targeted Database Searches of Mass Spectrometry Data: Implications for T-Cell Immunotherapies. J Proteome Res *16*, 1806-1816.

Ni, X., Tan, Z., Ding, C., Zhang, C., Song, L., Yang, S., Liu, M., Jia, R., Zhao, C., Song, L., et al. (2019). A region-resolved mucosa proteome of the human stomach. Nat Commun *10*, 39.

Parray, H.A., and Yun, J.W. (2015). Proteomic Identification of Target Proteins of Thiodigalactoside in White Adipose Tissue from Diet-Induced Obese Rats. International journal of molecular sciences *16*, 14441-14463.

Purcell, A.W. (2004). Isolation and characterization of naturally processed MHC-bound peptides from the surface of antigen-presenting cells. Methods Mol Biol *251*, 291-306.

Qin, S., Song, G., and Yu, Y. (2014). Phospholipid transfer protein in diabetes, metabolic syndrome and obesity. Cardiovascular & hematological disorders drug targets *14*, 149-153.

Taleux, N., Guigas, B., Dubouchaud, H., Moreno, M., Weitzel, J.M., Goglia, F., Favier, R., and Leverve, X.M. (2009). High expression of thyroid hormone receptors and mitochondrial glycerol-3-phosphate dehydrogenase in the liver is linked to enhanced fatty acid oxidation in Lou/C, a rat strain resistant to obesity. The Journal of biological chemistry *284*, 4308-4316.

Tzotzas, T., Desrumaux, C., and Lagrost, L. (2009). Plasma phospholipid transfer protein (PLTP): review of an emerging cardiometabolic risk factor. Obesity reviews : an official journal of the International Association for the Study of Obesity *10*, 403-411.

Zheng, Y., Qu, H., Xiong, X., Wang, Y., Liu, X., Zhang, L., Liao, X., Liao, Q., Sun, Z., Ouyang, Q., et al. (2019). Deficiency of Mitochondrial Glycerol 3-Phosphate Dehydrogenase Contributes to Hepatic Steatosis. Hepatology *70*, 84-97.